Clim Dyn (2013) 40:1569–1589
DOI 10.1007/s00382-013-1695-y

Impact of projected SST changes on summer rainfall in southeastern South America

C. Junquas · C. S. Vera · L. Li · H. Le Treut

Received: 23 November 2011 / Accepted: 4 February 2013 / Published online: 24 February 2013

Abstract Recent studies have shown that global warming and associated sea-surface temperature (SST) changes may trigger an important rainfall increase in southeastern South America (SESA) during the austral summer (December–January–February, DJF). The goal of this paper is to provide some insight into processes which may link global and SESA changes. For this purpose, a "two-way nesting" system coupling interactively the regional and global versions of the LMDZ4 atmospheric model is used to study the response to prescribed SST changes. The regional model is a variable-grid version of the global model, with a zoom focused over South America. An ensemble of simulations forced by distinct patterns of DJF SST changes has been carried out using a decomposition of full SST changes into their longitudinal and latitudinal components. The full SST changes are based on projections for the end of the twenty-first century from a multi-model ensemble of WCRP/CMIP3. Results confirm the presence of a major rainfall dipole structure, characterized by an increase in SESA and a decrease in the South Atlantic Convergence Zone region. Rainfall changes found in the WCRP/CMIP3 models are largely explained as a response of this dipole structure to the zonally-asymmetric (or longitudinal) component of SST changes. The rainfall response to the zonal-mean (or latitudinal) SST changes (including the global warming signal itself) shows an opposite contribution. The processes explaining the role of zonally-asymmetric SST changes involve remote effects of SST warming over the equatorial Indian and Pacific oceans inducing an atmospheric wave-train extended across the South Pacific into South America.

Keywords South America climate · Rainfall changes · Two-way nesting system · Sea surface temperature projections · Climate change

C. Junquas (✉) · L. Li · H. Le Treut
Laboratoire de Météorologie Dynamique,
Institut Pierre Simon Laplace, UPMC/CNRS, Paris, France
e-mail: junquas@cima.fcen.uba.ar

C. Junquas · C. S. Vera
Centro de Investigaciones Del Mar y la Atmosfera
(CIMA/CONICET-UBA), DCAO/FCEN, UMI IFAECI/CNRS,
Buenos Aires, Argentina

1 Introduction

The World Climate Research Program Coupled Model Intercomparison Project, phase 3 (WCRP/CMIP3) has provided a comprehensive set of climate simulations based on a wide range of future scenarios and on a large ensemble of general circulation models (GCM). Climate projections for the end of the twenty-first century, as deduced from those simulations, show in most cases a rainfall increase in the tropical regions, and a rainfall decrease in the subtropical regions (IPCC 2007). However, southeastern South America (SESA) is one of the few subtropical regions where simulations show in average, at the end of the twenty-first century, a significant rainfall increase during the austral summer (e.g., IPCC 2007; Vera et al. 2006b). This projection is consistent with the positive trend diagnosed from observations during the second half of the twentieth century, a signal resulting mostly from the warm season (Oct–March; Barros et al. 2008). SESA covers northern Argentina, Paraguay, Uruguay and southern Brazil, and includes La Plata Basin, the fifth largest basin in the world and the second in South America, after the Amazon basin. Improved knowledge of current and future rainfall variability in the basin has a high socio-economic relevance considering that more than 100 million people

live there, and local economies strongly depend on agricultural activities and hydroelectricity generation.

Recently, Junquas et al. (2012) analyzed climate projections for the twenty-first century provided by 18 WCRP/CMIP3 models, in order to explore physical mechanisms associated with the rainfall increase expected in SESA. They found that the projected rainfall trend for December–January–February (DJF) was positive in SESA but negative in southeastern Brazil, where is located the south Atlantic convergence zone (SACZ), a conspicuous feature of the South America Monsoon System (e.g., Vera et al. 2006a). They also found that this regional climate change is linked to a significant increase in the frequency of the positive phase of the leading pattern of summer rainfall variability. The pattern is characterized by a dipole-like structure with rainfall anomaly centers of opposite signs located in SESA and SACZ regions respectively (e.g., Doyle and Barros 2002). Although such result was evident in the 18-model ensemble, it showed a more coherent physical behavior in an ensemble of 9 models with a pronounced dipole structure, models that were retained for further analysis. In addition, Junquas et al. (2012) found that the positive phase of the rainfall dipole (associated with positive precipitation anomalies in SESA and negative ones in the SACZ region) was related to positive anomalies of sea surface temperature (SST) in the equatorial Pacific-Indian Ocean. Those SST anomalies favor the development of a Rossby wave-train pattern following an arch trajectory and linking the western equatorial Pacific and South America. The large-scale circulation favors in turn the regional development of an anticyclonic circulation anomaly located between SACZ and SESA, which promotes moisture convergence (divergence) and rainfall increase (decrease) in SESA (SACZ). The teleconnection induced by this Rossby wave-train appears as a key mechanism explaining the rainfall increase simulated by most of the models. A main objective of this study is to verify this hypothesis through sensitivity simulations performed with an atmospheric general circulation model reacting to prescribed SST conditions. In particular, we want to explore whether this wave-train mechanism is the main one explaining the projected rainfall change in SESA.

It is well known that positive SST anomalies in the equatorial Pacific during the warm phase of El Niño-Southern Oscillation (ENSO) induce positive rainfall anomalies over SESA (e.g., Paegle and Mo 2002; Grimm et al. 2000). However, due to complexity of processes involved, it is not clear yet how ENSO variability will evolve in response to a global warming (Collins et al. 2010). In addition, it is difficult to determine whether the SST changes identified in Junquas et al. (2012) as a plausible scenario for the twenty-first century, would primarily be due to changes in the mean conditions of the equatorial Pacific or would be related to changes in the patterns of equatorial SST variability, like ENSO. WCRP/CMIP3 simulations show that, as a consequence of the global warming associated with GHG increase, equatorial regions of the global ocean are affected by a stronger SST warming than the off-equatorial regions (e.g., Collins et al. 2010 and references therein). Moreover, SST changes induced by global warming include in particular warm anomalies in the equatorial Pacific (Collins et al. 2010; Fig. 2c). As a consequence, the development of Rossby wave-trains extending along the extratropical Pacific could be part of the atmospheric response to such patterns of SST increase. However, the whole complexity of the atmospheric mechanisms that could be induced by equatorial Pacific SST changes in a context of global warming, and therefore impact SESA rainfall, have not been deeply explored yet.

Previous studies have also evidenced links between the rainfall dipole variability in South America and the South Atlantic SST anomalies (e.g., Robertson and Mechoso 2000; Doyle and Barros 2002). In particular, the rainfall dipole positive phase has been associated with warm SST anomalies in the western subtropical South Atlantic (Doyle and Barros 2002). The equatorial Atlantic SST can also modulate the influence of ENSO over SESA rainfall during January–February. Through modeling sensitivity experiments, Barreiro and Tippmann (2008) showed that warm conditions in the equatorial Atlantic tend to weaken the influence of ENSO warm phase onto South America rainfall. As a consequence, SST changes in the Atlantic resulting from a global warming could also influence the rainfall response in SESA, directly or by modulating the equatorial Pacific teleconnection.

Addressing the complexity of all these interrelated processes requires a dedicated methodology. Sensitivity studies performed by a GCM are a common approach to address such issues. Gastineau et al. (2009) showed that many aspects of the global warming effect on large-scale circulation and precipitation can be reproduced by considering the projected SST changes as prescribed boundary conditions, while keeping constant both the sea-ice conditions and the GHG concentrations. Performing sensitivity tests with the IPSL-CM4 GCM (Marti et al. 2005), they showed that SST changes constitute a major driver of climate changes. Various works studied the influence of the CO_2 increase alone over the tropical precipitation (e.g., Allen et al. 2002; Sugi and Yoshimura 2004). However, Gastineau et al. (2009) found that in the IPSL model as in its atmospheric component LMDZ4, the only effect of the global SST changes (that is a consequence of the CO_2 increase) prevails over the direct effect of CO_2 increase. The purpose of this study is to perform sensitivity tests using different prescribed SST anomalies, and in particular a decomposition of the SST changes from the 9 models studied in

Junquas et al. (2012). The total SST changes are decomposed into a longitudinal component and a latitudinal one, following the methodology of Gastineau et al. (2009).

The longitudinal component of the SST changes (computed by the zonal asymmetry pattern) represents the differential heating between the tropical Pacific-Indian and the tropical Atlantic induced by climate warming. This longitudinal component seems relevant to the triggering of Rossby wave-trains extending throughout the south Pacific extratropics. This assumption will be examined and verified in the present work. Particular attention will be paid to the propagation of the wave-train and its influence on rainfall changes in SESA.

The latitudinal component of the SST changes is represented by the meridional profile of the zonal-mean SST changes. Gastineau et al. (2009) showed that this latitudinal component is by itself able to drive global changes in the atmospheric circulation strength and the zonal-mean precipitation changes. It is not known yet if the projected global-scale atmospheric changes induced by zonal-mean SST warming, like for example the slowdown of the tropical atmospheric circulation (Vecchi et al. 2006; Vecchi and Soden 2007; Gastineau et al. 2008), contribute to explain the projected rainfall increase in SESA. Therefore, another important aim of this study is to assess the influence of global-scale atmospheric circulation changes induced by zonal-mean SST warming over the austral summer rainfall in SESA.

Junquas et al. (2012) argued that the rainfall increase in SESA that has been identified in most of the models can be explained by a combination of large-scale and regional processes. For example, moisture flux convergence over SESA that can be promoted by large-scale circulation anomalies, is also strongly influenced by the presence of the Andes, a very high and narrow orographic barrier that is usually not well represented by global models (e.g., Vera et al. 2006a). There are some evidences that simulating the regional climate of South America with a resolution higher than that of the state-of-the-art GCMs could improve the representation of key processes related to precipitation. Refining the resolution in the region seems to improve the South American Monsoon System as it provides a better depiction of sea-land contrast and land surface feedbacks (e.g. Sörensson et al. 2010). In addition, a good representation of Andes orographic features is important for simulating low-level humidity fluxes from tropics to extratropics, which in turn is crucial for rainfall representation in SESA (e.g. Marengo et al. 2004; Xu et al. 2004). Previous studies also showed that the quality of the representation of the Andes could have influence over the south Pacific (e.g. the ITCZ and the SPCZ; Xu et al. 2004; Takahashi and Battisti 2007) that could in turn affect the precipitation in SESA via teleconnection processes.

In order to correctly simulate such spatial-scale interactions, we use in this study the atmospheric LMDZ4 model configured in the mode of "two-way nesting" (TWN), as used in Chen et al. (2011) for evaluating climate change related issues in eastern China. A TWN climate system relies on performing interactive simulations between a global atmospheric GCM and a regional climate model (RCM), representing a particular region with a finer spatial resolution than that in the GCM. Such system is able to integrate regional climate variability at finer spatial resolution into the GCM at global scale (Lorenz and Jacob 2005). In addition, there are indications that some systematic errors of the global circulation can be reduced globally by a more detailed representation of a particular region (Lorenz and Jacob 2005). By combining the RCM benefits (finer resolution) and the GCM benefits (global coverage), the TWN system seems an appropriate solution to represent teleconnection processes between regional and global climates.

The purpose of this paper is to perform a series of sensitivity numerical simulations using the TWN LMDZ4 climate model system, in order to identify the main mechanisms associated with the projected global SST changes that can explain the summer rainfall increase projected in SESA. We limit the study to two particular issues: (1) to identify which part of the projected SST changes is associated with teleconnection processes, and particularly the Rossby wave-train structure identified in Junquas et al. (2012), inducing positive trend in SESA rainfall, and (2) to understand if and how global-scale atmospheric processes linked to the zonal-mean SST changes influence climate in SESA.

The paper is organized as follows: Sect. 2 describes the model and data, and the performed simulations; Sect. 3 presents a validation of the TWN system in the control experiment; Sect. 4 discusses the sensitivity simulations forced by the projected SST changes, in terms of addressing regional rainfall changes in South America and in SESA particularly, and also by identifying underlying large-scale physical processes; Sect. 5 includes final discussion and conclusions.

2 Model and experiment

2.1 Model

The LMDZ4 model is the atmospheric component of the Institute Pierre Simon Laplace Coupled Model (IPSL-CM4; Marti et al. 2005). LMDZ4 is a grid-point model with a state-of-the-art physical package (Li 1999; Hourdin et al. 2006). The specificity of this atmospheric model is the possibility to stretch the horizontal spatial grid by

increasing the resolution in a particular region, and decreasing it outside ("zoomed" configuration). Two specific LMDZ4 configurations are used in this work: "LMDZ-global" with a horizontal grid of 96 × 72 points, uniformly distributed over the globe; and "LMDZ-regional" that is a zoomed version with global grid of 120 × 121 points. The zoom is centered over South America, allowing a regional horizontal resolution of about 100 km (Fig. 1). The two model configurations share the same physical parameterization and the same vertical discretization (19 hybrid levels), and only differ in their horizontal spatial resolution. Their main characteristics are summarized in Table 1. LMDZ-regional is used as a classic RCM, but it provides a better lateral-boundary treatment in comparison to a traditional limited area RCM. We use the TWN technique described by Lorenz and Jacob (2005; Fig. 1), by running in parallel LMDZ-regional and LMDZ-global and interactively coupling them together. The exchange of information (T, U, V, and Q) between the two models takes place every 2 h. As described in Chen et al. (2011), outputs of LMDZ-regional (LMDZ-global) are used as boundary conditions for LMDZ-global (LMDZ-regional) inside (outside) the zoomed domain. The TWN technique can improve feedbacks from regional climate to global climate, even in regions not covered by the two-way nesting.

Junquas et al. (2012) showed that, as in most of WCRP/CMIP3 models, the IPSL-CM4 model is able to reproduce the dipolar mode of precipitation variability in South America (described in the Introduction), and the physical mechanisms associated with summer SESA rainfall variability. However, IPSL-CM4 is one of the few models projecting by the end of the twenty-first century a decrease of rainfall in SESA. It remains then an open question why the rainfall change in SESA in response to the global warming is negative in IPSL-CM4, while it is positive in the majority of the WCRP/CMIP3 models. This question is out of the scope of this paper, but results will provide hypothesis that could answer it partly. The possible influence over the results of using this particular model will be discussed in the Conclusion section.

2.2 Design of experiments

The main characteristics of the performed sensitivity experiments are summarized in Table 2. Firstly the present DJF climate was simulated using the TWN technique (called CONTROL simulation). In CONTROL, climatological means of SST and sea ice distribution from the Atmospheric Model Intercomparison Project AMIP (Gates 1992) for the 1979–1999 period were considered as lower-boundary conditions for both LMDZ-global and LMDZ-regional. An ensemble of 30 runs was performed covering November to February. Each initial state is associated with the conditions of a distinct day generated by a random sampling from a meteorological sequence simulated by the model between October 20 and November 19. Each day of this sequence is then considered as a distinct state of November 1. In that sense, all the 30 members begin on November 1 but associated with a different initial state for both atmosphere and land surface conditions. Austral summer conditions are obtained from the multi-member ensemble DJF mean. November is considered as a month of "spin-up", to let the system the time to absorb the initial perturbation.

To assess the benefits of applying the TWN technique, a second experiment (called GLOBAL simulation) was performed running LMDZ-global alone under the same initial and boundary conditions as in the CONTROL simulation. It is evident that GLOBAL does not include potential feedbacks from the grid refinement over South America, since the TWN coupling is not performed in this case and only LMDZ-global with a uniform spatial grid configuration is run.

The next set of experiments was designed to explore climate changes induced by SST changes. Variations of

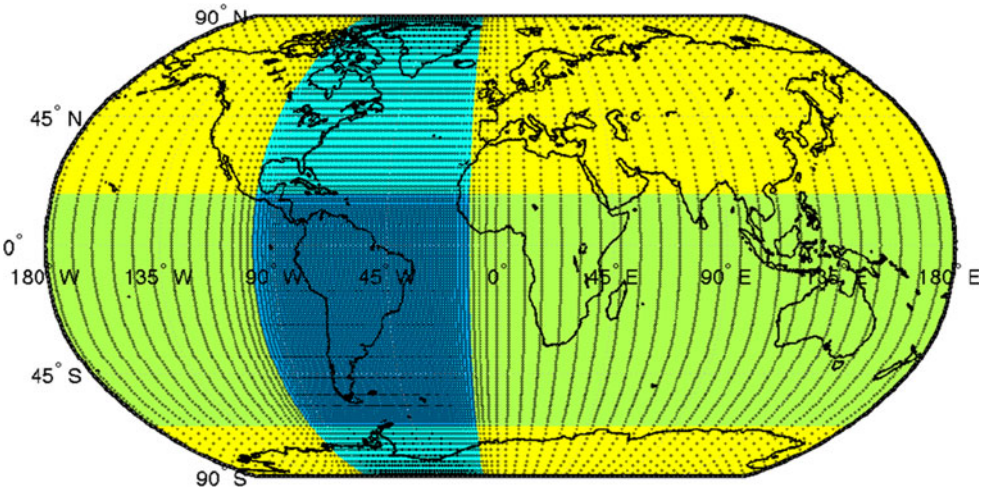

Fig. 1 Geographical representation of the LMDZ-regional grid-points. Regions where the latitude (longitude) resolution is reduced to 100 km is represented in *light green* (*light blue*). The zoomed region is in *dark blue*. *Yellow color* characterizes the rest of the globe

SST projected by the end of the twenty-first century were added to the observed mean SST considered in CONTROL. The SST changes correspond to those projected by the WCRP/CMIP3 9-model ensemble (MME) identified by Junquas et al. (2012; CCCMA T43, CCCMA T63, CSIRO, GFDL2.0, GFDL2.1, MIROC-hires, MIROC-medres, MIUB, UKMO HadCM3). They are defined as the seasonal DJF mean difference between 2079 and 2099 (from the Special Report on Emission Scenario A1B simulations) and 1979–1999 (from the twentieth century climate simulations). As explained in Introduction, the 9 models were identified by Junquas et al. (2012) as exhibiting the most common and coherent signal of summer rainfall projections in SESA for the end of the twenty-first century among a WCRP/CMIP3 18-model ensemble. These models were found as exhibiting a realistic representation of the leading pattern of summer rainfall variability in the present climate as in the future projections. In addition, the 9 selected models were identified as showing an increase along the twenty-first century of the frequency of the positive phases of the rainfall dipole-like pattern, in association with a positive trend of the rainfall DJF mean in SESA.

The spatial structure of SST changes used in this experiment, referred to as "FSST" (full SST change) hereafter, is plotted in Fig. 2a. A further sensitivity experiment, "ZSST" (zonal-mean SST change), was conducted adding only the zonal average of the SST changes (Fig. 2b) to the observed mean SST, in agreement with the method considered by Gastineau et al. (2009).

It is evident from Fig. 2b that the latitudinal component of the SST change exhibits the largest values at the Equator and the Northern Hemisphere mid-latitudes. Besides full SST changes (Fig. 2a) are mainly explained by its zonal average (Fig. 2b), the associated zonal asymmetries are not negligible, particularly in tropical regions (Fig. 2c), where the SST changes are large (Fig. 2a). The latter is particularly relevant in terms of atmospheric response, considering that the tropics exhibit the largest SST mean values. As discussed in Introduction, the study of the longitudinal component of full SST change is quite relevant to the purpose of this work, considering that zonal asymmetries in the tropical SST changes could induce asymmetries in the tropical diabatic heating sources with consequences in the response of the extratropical circulation in the southern hemisphere (SH). The corresponding change, called "ASYM" (asymmetric SST change), can be assessed by analyzing the differences between FSST and ZSST.

Various studies found that the radiative effect of the GHG increase alone, without SST changes, induces a reduction of the tropical precipitation (e.g. Allen et al. 2002; Sugi and Yoshimura 2004). In particular, Allen et al. (2002) showed that in atmospheric simulations forced by only SST changes, without GHG increase, the hydrological cycle increases to compensate the missing GHG radiative heating. However, Gastineau et al. (2009) showed that the tropical rainfall changes induced by the missing radiative effect of GHG increase are much smaller than those changes induced by the SST increase alone. When both GHG and SST increase are considered, as in the real-world global warming, tropical precipitation increases due to the dominant effect of SST increase (Sugi and Yoshimura 2004). Moreover, Gastineau et al. (2009) found that the forcing by zonal-mean meridional SST changes is necessary (and sufficient) to correctly simulate projected changes in large-scale atmospheric circulation and zonal mean precipitation. In that sense, as it was explained in Introduction, the main purpose of this paper is to study mechanisms associated with SST variations. However, in order

Table 1 Main characteristics of LMDZ-global and LMDZ-regional operating under the configuration of two-way nesting (TWN)

	LMDZ4-global	LMDZ4-regional
Horizontal resolution inside the zoomed region	2.5° × 3.75°	1° × 1°
Horizontal resolution outside the zoomed region	2.5° × 3.75°	2.6° × 8°
Number of points (lon × lat)	96 × 72	120 × 121
Center of the zoom		55°W;22.5°S
Extension of the zoom		82.8°E–W;82.8°N–S
Time step of the physics	30 min	30 min
Time step of the dynamics	3 min	40 s
Physical parametrization	LMDZ4	LMDZ4

Table 2 Summary of the acronyms used in the text, including the performed experiments (bold) and ASYM (italic)

For experiments, the use of the two-way nesting (TWN) method means that LMDZ-global and LMDZ-regional are run in parallel (see Sect. 2.1)

Acronym	Method/definition	Sea surface temperature	Ensemble size	CO_2 value (ppm)
CONTROL	TWN	Climatological average over 1979–1999	30	348
GLOBAL	LMDZ-global alone	Climatological average over 1979–1999	30	348
FSST	TWN	Full future SST changes added	30	348
FSSTG	TWN	Full future SST changes added	30	696
ZSST	TWN	Zonal mean of future SST changes added	30	348
ASYM	FSST minus ZSST			
ASST	TWN	Full minus zonal future SST changes added	30	348

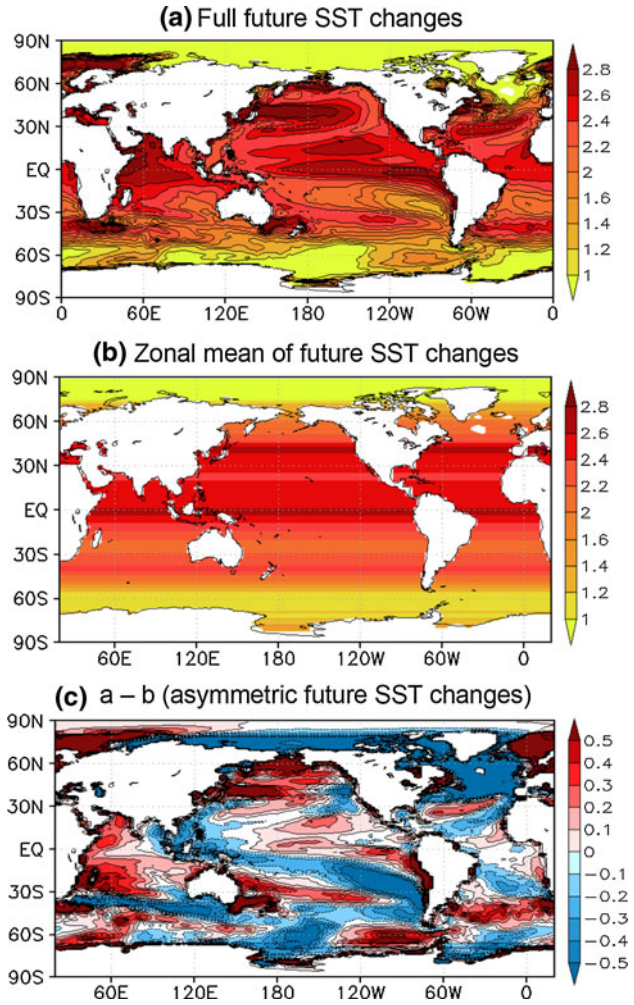

Fig. 2 **a** Sea surface temperature (SST) changes (K) for December–January–February (DJF) between present-day climate (1979–1999) and the end of the twenty-first century (2079–2099), projected by 9 WCRP/CMIP3 models listed in Sect. 2.2 (under SRES-A1B scenario). **b** Zonal average of the SST changes displayed in **a**. *Color scale* interval is 0.2 K. **c** Difference between **a** and **b**. *Color scale* interval is 0.1 K

to verify that the GHG increase effects would not significantly influence the SESA precipitation changes, we performed an additional experiment, called "FSSTG", considering CO_2 increase in the atmosphere. FSSTG is the same experiment as FSST, except that the CO_2 concentration in the atmosphere was increased to the double level of its initial value in FSST (696 ppm instead of 348 ppm).

3 Model validation

The ability of the TWN LMDZ4 model system to reproduce the DJF climate of South America is first evaluated. The model assessment is made at large (regional) scale, comparing the LMDZ-global (LMDZ-regional) outputs of CONTROL simulation, performed under the TWN configuration, with observed and reanalyzed data. Rainfall monthly mean fields from the Climate Prediction Center Merged Analysis of Rainfall (CMAP) dataset (Xie and Arkin 1997) and from the recent version 2.2 of the Global Precipitation Climatology Project (GPCP; Huffman et al. 2011) are used to describe the rainfall observed in austral summer between 1979 and 1999. The 20-year reanalysis dataset ERA-Interim (Simmons et al. 2006) from the European Centre for Medium-Range Weather Forecasts (ECMWF) is used to describe observed fields of humidity flux, velocity potential and geopotential height. Humidity fluxes are computed from the wind components and specific humidity fields and they are vertically integrated between 1,000 and 300 hPa, following the method employed in other studies (e.g., Labraga et al. 2000; Doyle and Barros 2002).

3.1 Large scale

The DJF climatological mean conditions resulting from the ensemble mean of the 30 LMDZ-global runs from the CONTROL simulation are compared to the corresponding observed climatological means. Figure 3a, b show the large-scale DJF mean precipitation depicted by CMAP data (for the period 1979–1999) and by the model, respectively. The Inter-tropical convergence zone (ITCZ) is well simulated by the model in the Atlantic as well as in the Pacific. The three tropical regions of active convection: equatorial Indian-west Pacific sector, tropical South America, and central Africa (e.g., Krishnamurti et al. 1973; Chen et al. 1999), are evident in the simulations, although they are more intense and located further north in the model than observed. In particular, simulated mean precipitation over South America exhibits the observed maximum over the Amazon region linked to the SACZ that extends into the southwestern Atlantic. The region of maximum mean precipitation related to the South Pacific Convergence Zone (SPCZ) is simulated stronger and somewhat detached from the equatorial rainfall band extended along the Equator in the Indian-western Pacific Oceans. In addition, simulations exhibit less precipitation over Indonesia and northern Australia, and more precipitation over the western Indian Ocean than observed.

Mean fields of velocity potential and divergent wind at the 200-hPa level are also validated in order to assess the model ability in representing the divergent circulation forced by the tropical diabatic heating (e.g., Krishnamurti et al. 1973; Tanaka et al. 2004). Three zones of minimum potential velocity or maximum divergence associated with the regions of maximum mean precipitation (Fig. 3a) are evident in the reanalysis, with maximum convergence regions over the eastern equatorial sectors of both the

Pacific and Atlantic Oceans (Fig. 3c). The model seems to reproduce the main features of the divergent circulation in the tropics although with some limitations (Fig. 3d). In particular, the model is able to represent the upper-level divergence associated with both the Amazon and SACZ convection in South America, although it has some deficiencies in representing the intensity and location of the upper-level convergence observed at the subtropics. In addition, the simulated upper-level divergence over Indonesia and northern Australia is weaker or even of opposite sign than observed, consistently with the errors found over those regions in the simulated mean precipitation (Fig. 3b).

3.2 Regional scale

Observed DJF mean fields of precipitation and humidity are used to validate the LMDZ-regional outputs of CONTROL over South America (Fig. 4). The DJF climatological mean precipitation computed from CMAP and GPCP datasets are depicted in Fig. 4a, b respectively while Fig. 4c displays the corresponding simulated field. The model is able to reproduce the general features of summertime rainfall, like the precipitation maximums over the Amazon, Atlantic ITCZ and SACZ regions. The model tends, however, to simulate a weaker Atlantic ITCZ and more precipitation and shifted northwestward than observed in the Amazon basin. It is worth to mention that large differences, particularly in precipitation intensity, are also observed between CMAP and GPCP. It is known that the lack of reliable precipitation datasets over South America limits precipitation validation of any model in the region (e.g., Vera et al. 2006b).

Model precipitation biases are large and positive over the Brazilian plateau in association with the SACZ (Fig. 4). A similar bias was described by Codron and Sadourny (2002) that used a previous version of the LMD AGCM to represent the climate in South America. They associated this bias with an overestimated orographic precipitation and were able to reduce it by 20 %, improving the water vapor advection scheme in the model. On the contrary, to the south of SESA and in Northeastern Brazil, negative precipitation biases are found. In addition, the simulation seems to overestimate precipitation along the Andes Mountains. Although, precipitation gridded datasets are deficient in representing the right precipitation amounts observed along the Andes (Vera et al. 2006b). Climatological mean precipitation fields computed by Hoffman (1975) from more than 1,700 stations, exhibits a precipitation maximum along the tropical Andes that is not represented in the available precipitation gridded datasets and it is not that dissimilar to that simulated by the model.

Table 3 shows metrics for the precipitation reproducibility in both all South America and SESA. The model shows significant positive correlation and small RMSE values when compared with both GPCP and CMAP. The model tends however to show a precipitation pattern closer to GPCP than CMAP, with values of spatial correlation higher and closer mean values in both South America and SESA.

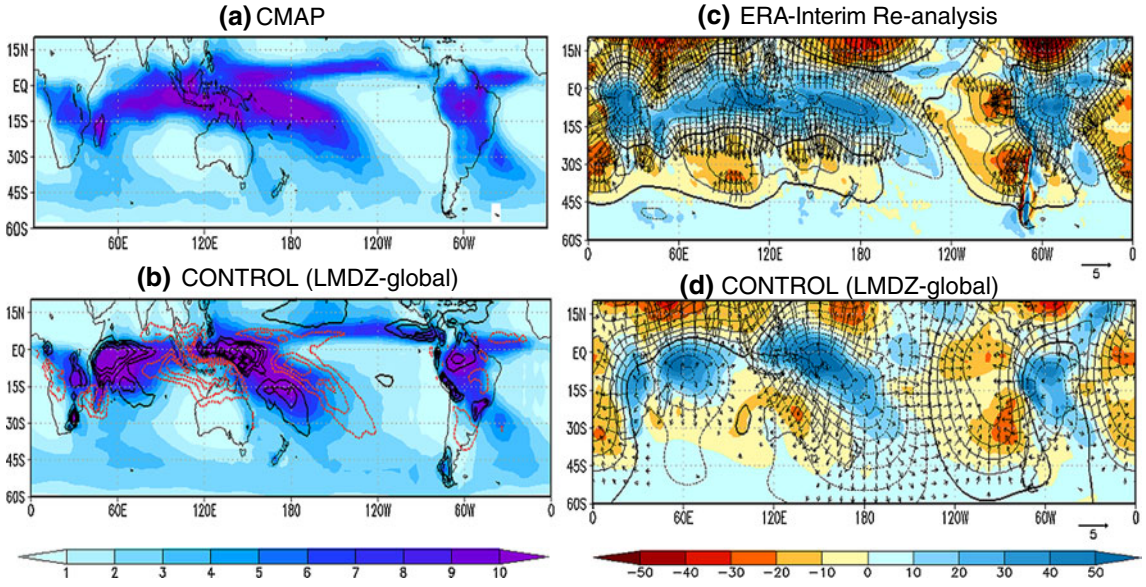

Fig. 3 DJF mean of **a** and **b** Precipitation (mm/day), **c** and **d** 200-hPa velocity potential (*contour*, interval is 10×10^5 m^2 s^{-1}), 200-hPa divergent wind (*arrows*, units m s^{-1}), and 200-hPa divergence (*shade*, interval is 10×10^7 s^{-1}). Data are from **a** CMAP for the period 1979–1999, **c** ERA-interim re-analysis for the period 1989–2009, **b** and **d** the LMDZ-global outputs of the CONTROL simulation. *Contours* in **b** indicate the **b**–**a** difference (interval 1.5 mm/day, *zero contour omitted*, *positive* values in *black*, *negative* values in *red*)

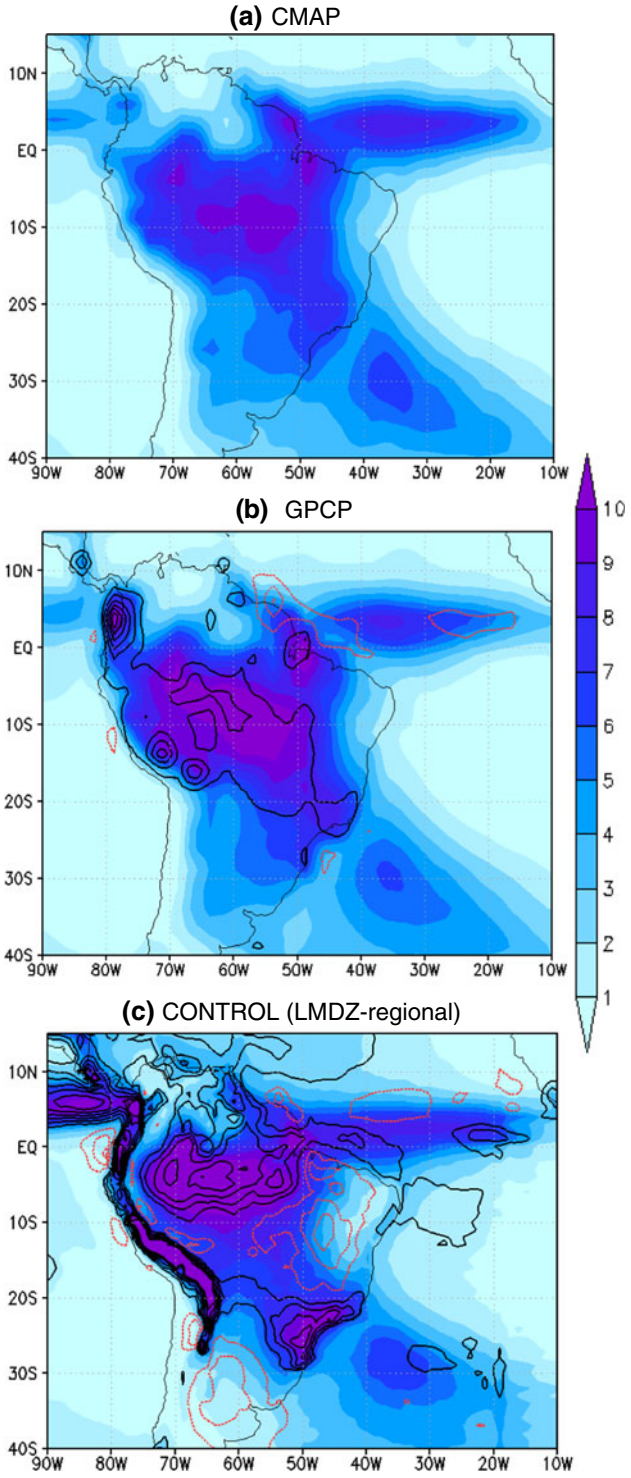

Fig. 4 Mean precipitation (mm/day) in DJF from **a** CMAP, **b** GPCP, and **c** LMDZ-regional in the CONTROL experiment. *Contours* in **b** (**c**) indicate the **b**–**a** (**c**–**a**) difference (interval 1 mm/day, *zero contour omitted*, *positive* values in *black*, *negative* values in *red*)

Vertically-integrated mean moisture flux and its associated divergence, computed from both reanalysis data (Fig. 5a) and CONTROL simulation (Fig. 5b) are also compared. The model simulates the general features of the continental-scale anticyclonic circulation that characterizes mean humidity fluxes in tropical South America (e.g., Vera et al. 2006a). However, moisture fluxes along the western branch of the gyre exhibit over Paraguay and west of Brazil a dominant southward direction in the reanalysis (Fig. 5a), while the simulated ones display a more southeastward orientation, merging over the Brazilian plateau with the fluxes emanating from the western branch of the South Atlantic anticyclone (Fig. 5b). This particular flux bias seems associated with the mean precipitation positive bias exhibited by the model over that region (Fig. 4c). A vertical cross section at 17°S of observed meridional humidity fluxes (Fig. 5c) shows the distinctive low-level maximum along the eastern slopes of the Andes in association with the South America low-level jet (LLJ) that intensifies over that region (e.g., Vera et al. 2006a). Also, a secondary low-level maximum is clear in the reanalysis off the eastern coast of South America associated with the western branch of the South Atlantic anticyclone. Figure 5d shows that the model is able to represent both structures. Nevertheless, the simulated maximum along the Andes slope is stronger and extends eastward when compared to reanalysis data, while the moisture flux maximum located off the eastern coast is simulated weaker than observed.

3.3 Assessment of the TWN method in South America

The TWN method is assessed by comparing the LMDZ-global outputs of the CONTROL simulation with those of the GLOBAL simulation performed without TWN technique (Table 2). Both LMDZ-global outputs share the same horizontal resolution. However, in the GLOBAL experiment LMDZ-global is run alone, while in the CONTROL experiment it is run in parallel with LMDZ-regional. Consequently, the assessment focuses in determining the influence of the high-resolution information transferred from the regional model under the TWN technique in CONTROL, since this transfer is absent in GLOBAL. Figure 6 shows that the main regional climate structures are better represented in CONTROL, performed using the TWN technique. In particular, the intensity and location of the precipitation associated with the ITCZ, Amazon and SACZ regions are better simulated in CONTROL (Fig. 6a) than in GLOBAL (Fig. 6b). Furthermore, the maximum regions of precipitation associated with ITCZ and Amazon are merged in the GLOBAL simulation (Fig. 6b), which exhibits a more intense ITCZ than observed (e.g. Fig. 4a). On the other hand, CONTROL clearly shows two distinct maximum centers of precipitation (Fig. 6a). It is noticeable though that the orographic precipitation bias identified in the LMDZ-regional outputs of CONTROL (Fig. 4c) is accentuated in the LMDZ-global outputs by the use of the

Table 3 Mean value, spatial correlation and relative RMSE (%) of the precipitation averaged in SESA (32°S:25°S,60°W:50°W) and/or South America (40°S:5°N, 90°W:10°W) for the CONTROL experiment (LMDZ-regional outputs), CMAP and GPCP datasets

	Mean value (mm/day)		Spatial correlation (South America)		Relative RMSE (%) (South America)	
	SESA	South America	CMAP	GPCP	CMAP	GPCP
CONTROL (LMDZ-regional)	5.4	4.5	0.85	0.87	25.7	25.5
CMAP	5	4	1	0.97	0	12.7
GPCP	5.5	4.3	–	1	–	0

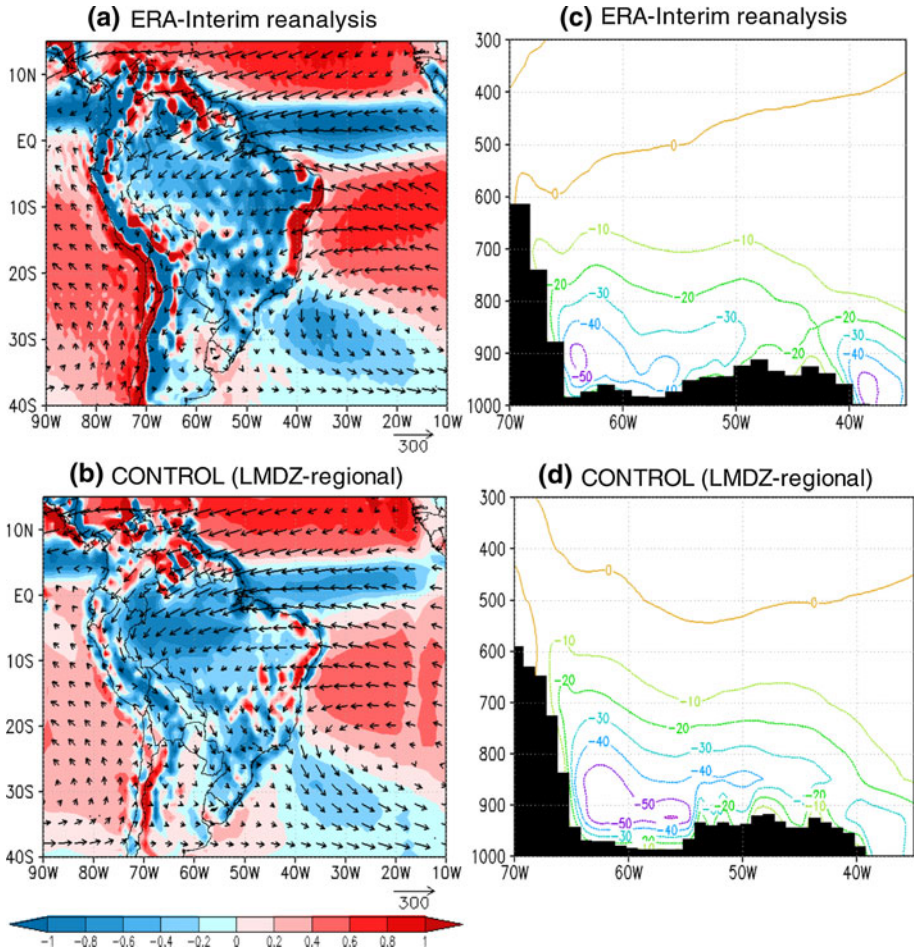

Fig. 5 DJF vertically-integrated moisture fluxes (*arrows*) and its divergence (*contour*) from **a** ERA-Interim Reanalysis, and **b** LMDZ-regional outputs of the CONTROL simulation. *Color* scale interval of divergence is 0.2 kg m^{-2} s^{-1}. Reference vector of 300 kg m^{-1} s^{-1} is displayed at the *lower right corner*. *Vertical* section at 17°S of the meridional component of the moisture flux from **c** ERA-Interim Reanalysis, and **d** LMDZ-regional outputs of the CONTROL simulation. *Contour* interval is 10 kg m^{-1} s^{-1}

TWN technique probably due to the finer resolution considered in this experiment. However, considering quantitative dispersion values like spatial correlation and relative RMSE, the observations indicate a South American precipitation pattern closer to CONTROL than to GLOBAL (not shown). Regarding the moisture transport, the GLOBAL simulation (Fig. 6d) shows evidences of a single low-level maximum of moisture transport (between 50 and 60°W), while a second relative maximum located over the Atlantic Ocean at around 38°W is depicted in both CONTROL (Fig. 6c) and reanalysis (Fig. 5c). CONTROL seems then able to represent both the maximum along the Andes, and that off the eastern coast (Fig. 6c).

4 The effect of SST change

The sensitivity of the TWN LMDZ4 runs to SST changes (as described in Sect. 2.2; Table 2) is analyzed in this section. The purpose of this study is to examine the mechanisms associated with different structures of SST changes and their influence over the SESA rainfall and the associated large-scale atmospheric circulation. There are three main atmospheric responses considered in the SST related forcing: (1) that associated with full SST changes depicted in FSST simulations (2) that associated with zonal-mean SST changes described by ZSST simulations, and (3) that associated with zonally-asymmetric SST

changes depicted by ASYM (considered as the difference of FSST minus ZSST). Details of the numerical experiments are described in Table 2. Changes are represented as the differences of each of these simulations with CONTROL.

4.1 Full SST change responses

As mentioned in Sect. 2.2, simulations are performed under constant GHG concentration values, since SST fields are the only modified boundary conditions. Gastineau et al. (2009) already showed that such simulations with LMDZ4 reasonably reproduce the main features of global warming, such as changes in tropical precipitation and dry static stability. In this section, we will firstly check the validity of this statement in our model configuration by comparing few basic features in FSST simulations with those of WCRP/CMIP3 coupled runs under the A1B scenario, in terms of large-scale atmospheric circulation. Then, the full SST changes responses will be analyzed in terms of regional precipitation changes in South America by comparing FSST with FSSTG, which besides the SST changes includes CO_2 concentration increase in the atmosphere (Table 2).

Large-scale precipitation changes, associated with FSST simulation, are presented in Fig. 7a. The main global-scale changes in the southern hemisphere correspond to increases in the tropics and mid latitudes, and decreases in the subtropics, in agreement with the projections by WCRP/CMIP3 models (e.g., IPCC 2007). The large-scale atmospheric circulation changes are described by 200-hPa potential velocity and divergent wind (Fig. 7b), following Tanaka et al. (2004) and Gastineau et al. (2009). FSST shows large-scale circulation changes coherent with the corresponding global rainfall changes, with three upper-level divergence (convergence) anomalies located at the tropical regions with positive (negative) rainfall changes. Chen et al. (1999) showed that DJF tropical-subtropical circulation in the SH, is largely dominated by a combination of a long-wave regime associated with a one-wave pattern maintained by the heating over the tropical Indo-Pacific, and a short-wave regime associated with 2–6 wave patterns essentially forced by the convection over South America, Africa, and tropical Indian Ocean. Figure 7b shows a three-wave pattern, resembling those of the short wave regime described by Chen et al. (1999). It shows a general slowdown of the tropical divergent circulation, in agreement with future projection from most of the coupled models (e.g., Gastineau et al. 2009).

Changes in the zonal mean meridional streamfunction resulted from FSST (Fig. 7c) are also analyzed to assess modifications in the global Hadley cells (Gastineau et al. 2008). Positive (negative) streamfunction centers

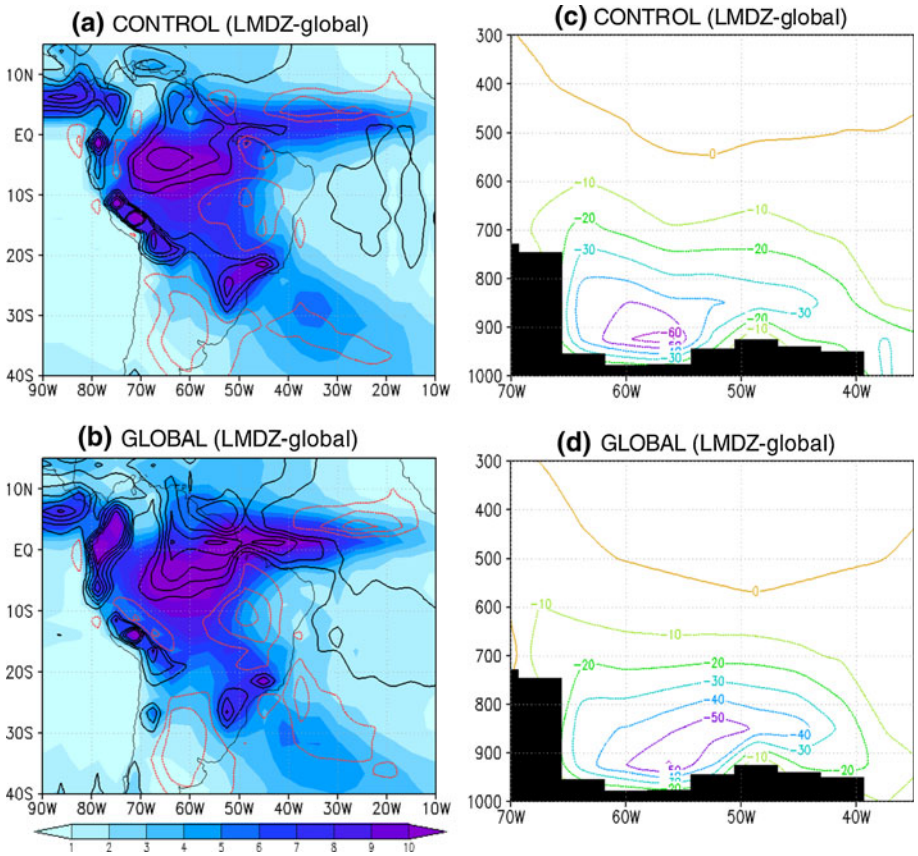

Fig. 6 Simulated precipitation (mm/day) in **a** and **b**, and vertical section at 17°S of moisture flux (kg m^{-1} s^{-1}) in **c** and **d**. **a** and **c** from LMDZ-global outputs of the CONTROL experiment, and **b** and **d** are results of the GLOBAL experiment (LMDZ-global alone). *Contours* in **a** (**b**) indicate the difference between Figs. 4a and 6a (6b) (interval 1 mm/day, *zero contour omitted*, *positive* values in *black*, *negative* values in *red*)

correspond to clockwise (counterclockwise) circulation. The dominant structure in CONTROL (represented in black contours in Fig. 7c) is the strong winter Hadley cell with the ascent branch located at about 5°S and the subsidence zone at about 30°N. Between 10°S and 30°S, the summer Hadley cell is visible, but much weaker than the winter cell. Circulation changes associated with FSST (represented in shaded in Fig. 7c) show a negative anomaly center located over the CONTROL winter Hadley cell at about 5°N (Fig. 7c), resulting in a weakening of the winter Hadley cell. If we focus on the differential circulation (shading in Fig. 7c), we can then observe a pair of cells between 25°S and 35°N with the ascending branch near 5–10°N. The two descending branches at 25°S and 35°N are coincident with the descending branches of the two Hadley cells in the basic flow. Such a situation can be interpreted as an enhancement of subsidence at 25°S and 35°N respectively. Also, positive meridional streamfunction anomaly changes at about 250 hPa and 15°N indicate an upward extension of the Hadley cell, and an increase of the tropical tropopause height, which is a common feature found in global warming projections (Lu et al. 2007). A poleward shift of the winter cell is also clear, characterized by a positive anomaly center at about 20°N–30°N (the subsiding branch of the winter cell), and a negative center between 20°S and 5°N (the ascending branch of the winter cell). In agreement, Fig. 7d shows an increase of the precipitation over the winter cell ascending branch. These changes are in agreement with the global warming projections of the WCRP/CMIP3 models, showing a weakening of the large-scale atmospheric circulation, a general slowdown of the Hadley cell (Vecchi et al. 2006; Vecchi and Soden 2007; Gastineau et al. 2008), a poleward shift of the winter Hadley cell (Lu et al. 2007), and a zonal mean precipitation increase in the ascending branch (Chou and Neelin 2004). It seems that FSST simulation is able to represent the main global signals, when only SST changes are imposed to the model. This result is important, since it indicates that physical processes revealed in such SST change sensitivity tests are close to those involved in a global warming scenario.

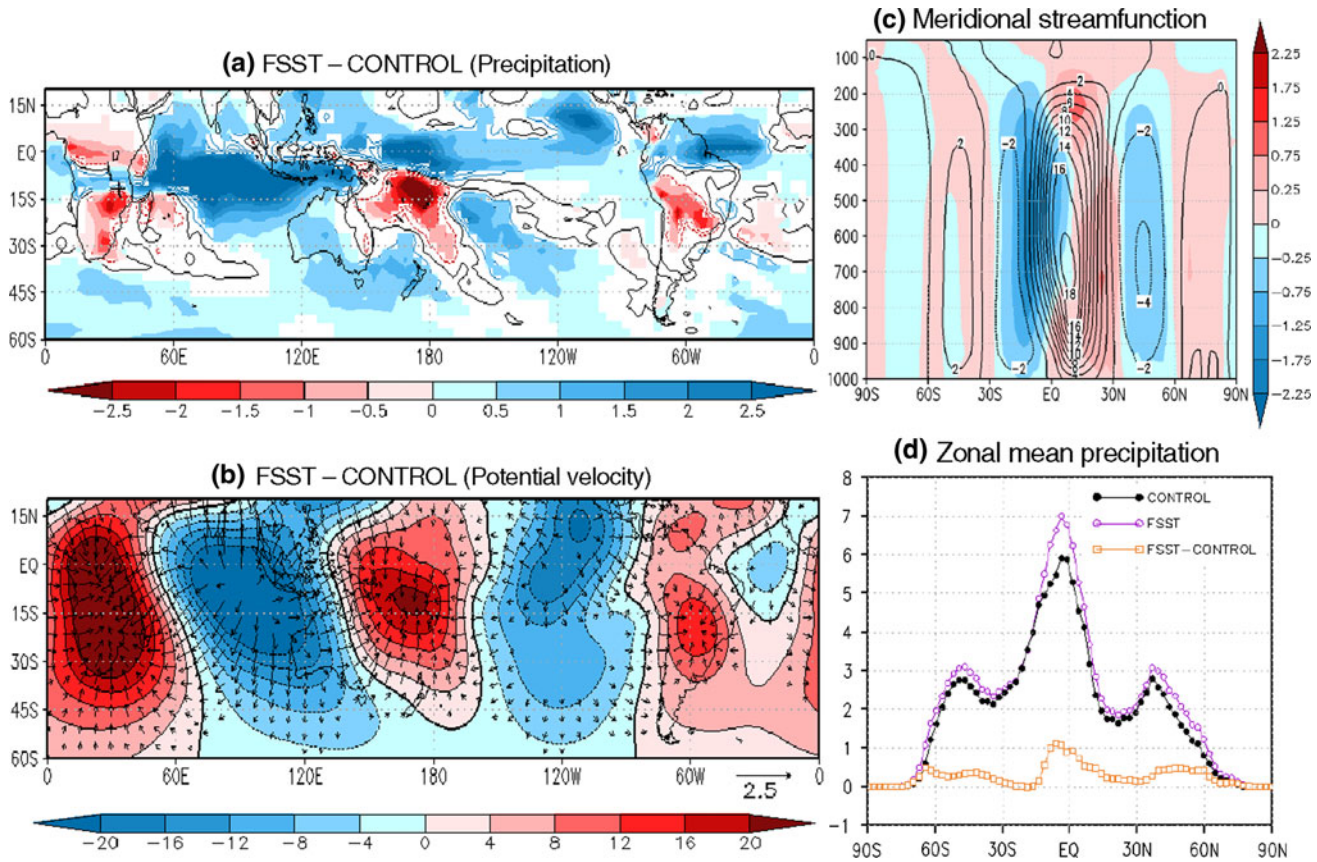

Fig. 7 Global anomalies from LMDZ-global corresponding to the difference between FSST (the full SST change simulation) and CONTROL for **a** Precipitation (mm/day), *positive* (*negative*) significant values at 90 % of the student test are shaded in *blue* (*red*) and the 0 level is in bold dark, **b** 200-hPa velocity potential (*contour* and *color*, interval 4×10^5 m^2 s^{-1}, *black contour* indicates the 0 level) and divergent wind (vectors, reference vector is displayed at the *lower right* corner in m s^{-1}), **c** meridional streamfunction (*shaded* with a *color* scale interval of 0.25 10^{10} kg s^{-1}). The meridional streamfunction of the CONTROL experiment is represented in *black* contours with an interval of 2.10^{10} kg s^{-1}. **d** Zonal mean precipitation of the CONTROL simulation (*black line*), FSST (*violet line*) and the FSST minus CONTROL difference (*orange line*)

At regional scales, rainfall changes resulted from FSST simulations over South America are displayed in Fig. 8a. Rainfall increases at the Atlantic ITCZ, over northern South America comprising the northern SACZ region, and southern SESA while it decreases over central South America. Rainfall changes resulting from FSSTG (Fig. 8b) show same structures in the subtropics than those from FSST (Fig. 8a), although with stronger rainfall decrease in central South America. Weak and insignificant (not shown) differences between FSSTG and FSST indicate that adding CO_2 concentration increase in the experiment has no significant influence over the SESA precipitation changes. However, in the tropics the increased Atlantic ITCZ precipitation is significantly reduced when the CO_2 increase is simulated, which is coherent with results of previous studies (e.g. Allen et al. 2002; Sugi and Yoshimura 2004).

The regional influence of CO_2 concentration increase is then analyzed in terms of regional humidity transport. FSST shows a weakening of the continental moisture transport from tropics to subtropics (Fig. 8e) and consequently a decrease of moisture transported from the Amazon basin to SESA. Furthermore, the increased convection in the ITCZ region is associated with stronger trade winds enhancing the South Atlantic subtropical anticyclone. The moisture transport from the subtropical anticyclone into the continent is then increased, and a positive rainfall anomaly is found over the northern part of the SACZ region, as well as in the oceanic part of the SACZ. From 20°S to 30°S and east of the Andes, a southward moisture transport anomaly is depicted, associated with a weak convergence anomaly over the coastal part of SESA. When the CO_2 concentration increase in the atmosphere is also included (FSSTG; Fig. 8f), the humidity transport from tropics to subtropics seems to be increased, but it does not affect significantly SESA where the structural rainfall changes remain essentially similar. The differences between FSSTG and FSST have also been analyzed in terms of large-scale teleconnections, and results did not reveal significant changes that might influence the SESA precipitation (not shown).

The regional FSST responses presents some differences with the precipitation changes projected by WCRP/CMIP3 MME (Fig. 11.15, Christensen et al. 2007), which show on average a large precipitation increase over subtropical SESA until 20°S and negligible changes to the north. We can tentatively conclude that regional rainfall changes projected for South America in a context of global warming might be the consequence of more complex processes particularly at regional scale. Nevertheless, it is evident that the rainfall changes obtained from FSST capture the essential features of the projected rainfall changes by WCRP/CMIP3, and they are thus useful for a further analysis of the physical mechanisms involved.

4.2 Rainfall responses to zonal-mean and asymmetric SST changes

Climate responses resulted from ZSST to ASYM are analyzed in this section. Figure 8c shows that rainfall change patterns in South America related to ZSST are similar to those for FSST (Fig. 8a). On the other hand, the ASYM difference is essentially characterized by a rainfall increase over subtropical SESA until around 22°S, and rainfall decrease in the SACZ region and northeastern South America (Fig. 8d). The rainfall changes described by the three numerical configurations are further analyzed along the A–B transect drawn in Fig. 8a, extended along the eastern coast with a SW-NE orientation. Rainfall changes associated with the southern transect portion represent those in SESA, while rainfall changes at the northern transect part represent those of the SACZ region. The analysis (Fig. 9) confirms that ZSST and ASYM represent opposite rainfall anomaly behavior in SESA and SACZ regions. ZSST shows rainfall decreases over subtropical SESA with values as low as −1.5 mm/day, and rainfall increases in the SACZ region. On the other hand, ASYM shows increases in SESA with values of around 0.8 mm/day and decreases over the SACZ region with values of about −0.5 mm/day. The response associated with FSST is clearly a combination of those associated with both ZSST and ASYM: weak increases in the extratropical portion of SESA, large decreases in the subtropics including the southern SACZ region, and increases in the tropical portion, including the northern SACZ region.

As it was mentioned in Sect. 2.2, we performed 30 members for all the numerical experiments. Figure 10 shows box-and-whisker plots on the dispersion of precipitation simulations for each experiment. Performing a regional average in SESA, it is clear that the dispersion among the 30 members is large, particularly for FSST. Figure 10 also reveals some overlapping between the SESA rainfall mean values simulated by ZSST and those simulated by FSST. However, the median in FSST is at a similar level of the upper quartile in ZSST. The latter indicates that the rainfall increase in ASYM (obtained by FSST-ZSST; cf. Fig. 9) is significant.

The large-scale rainfall patterns associated with both ZSST and ASYM are further explored. Global precipitation changes associated with both experiments (Fig. 11) seem directly related to their corresponding SST forcing (Fig. 2), with areas of precipitation increase mainly located in tropical regions of large positive SST changes, in agreement with Gastineau et al. (2009). Changes induced by ZSST (Fig. 11a) are characterized by a general precipitation increase in the tropical band where SST changes are large (Fig. 2b), and a decrease in the subtropics. Tropical rainfall increase seems particularly large over the Indian,

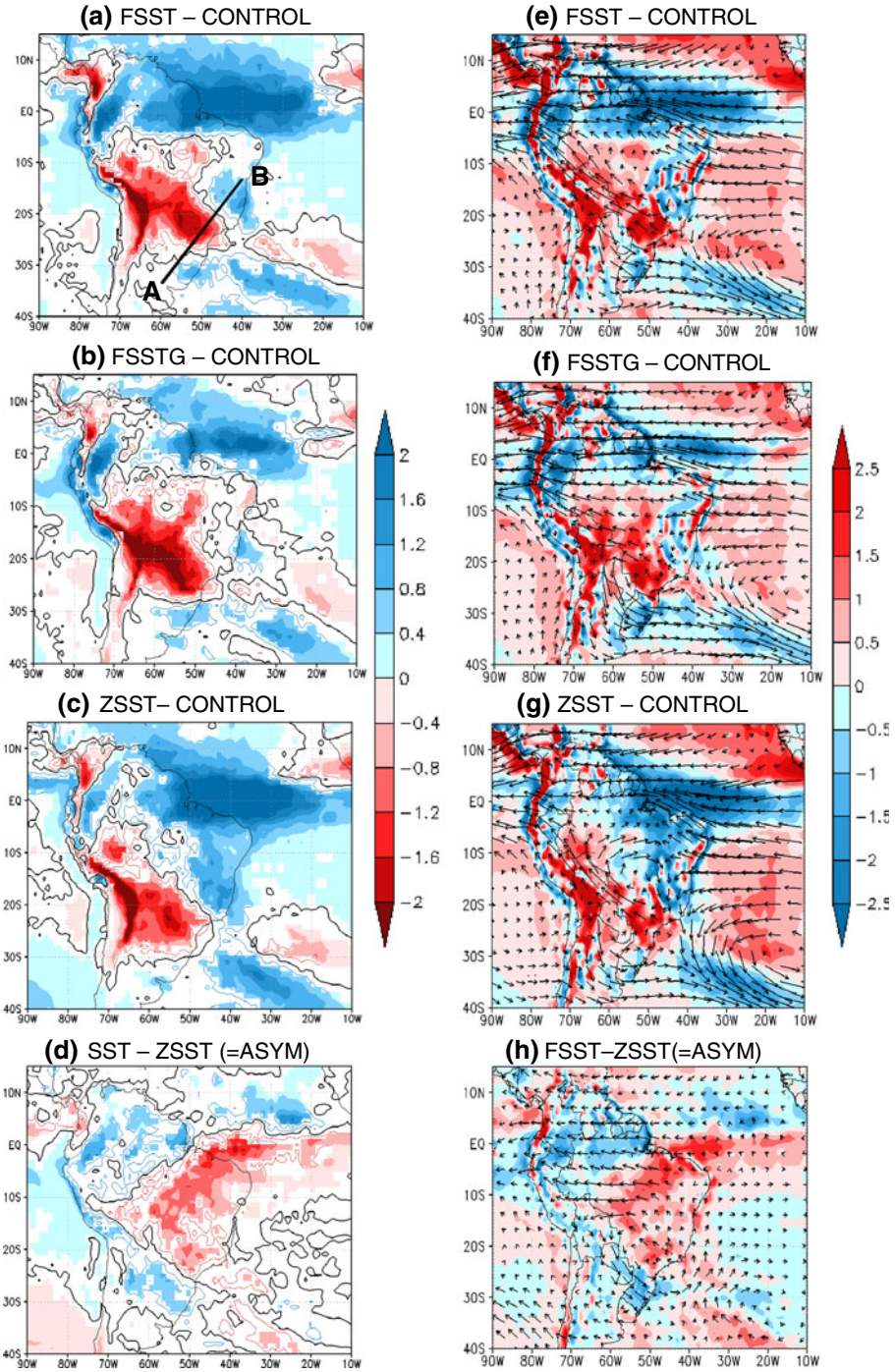

Fig. 8 *Left panels* Regional rainfall anomalies (mm/day, from LMDZ-regional model) corresponding to **a** FSST minus CONTROL, **b** FSSTG (the combined full SST changes and CO_2 increase simulation) minus CONTROL, **c** ZSST (the zonal-mean SST change simulation) minus CONTROL, and **d** ASYM (the difference FSST minus ZSST). *Positive* (*negative*) significant values at 90 % of the student test are shaded in *blue* (*red*). The 0 level is in *bold dark*. The **a**–**b** transect in **a** is used to represent the transect of Fig. 9. *Right panels* Anomalies of vertically-integrated (1,000–300 hPa) moisture flux (*arrows*) and its divergence (*shaded*) from outputs of LMDZ-regional for **e** FSST minus CONTROL, **f** FSSTG minus CONTROL, **g** ZSST minus CONTROL, **h** ASYM. *Color* scale interval for the divergence is 0.5×10^{-5} kg m^{-2} s^{-1}. Reference vector of 30 kg m^{-1} s^{-1} is displayed at the *lower right corner*

and western equatorial Pacific (Fig. 11a) where maximum mean SSTs locate (not shown). Large rainfall decreases are found over the southwestern tropical Indian Ocean, southwestern tropical Pacific Ocean, and central South America, being the three regions located to the southwest of the three maximum rainfall increase equatorial zones, respectively. On the other hand, ASYM displays distinctive positive changes over the southern tropical Indian Ocean, northern Australia, and the central equatorial Pacific ocean (Fig. 11b), corresponding to regions of positive zonally-asymmetric SST change (Fig. 2c).

4.3 Atmospheric circulation responses to zonal-mean and asymmetric SST changes

Both large-scale and regional atmospheric circulations are analyzed in this section for ZSST and ASYM in order to better understand the physical mechanisms linking the SST

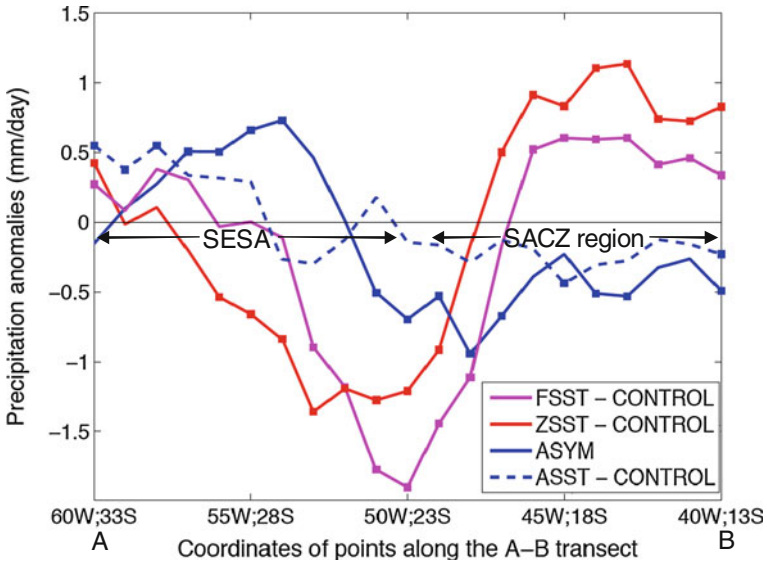

Fig. 9 Rainfall anomalies from the LMDZ-regional outputs of each simulated anomalies considered computed along the **a**–**b** transect indicated in Fig. 8a. FSST minus CONTROL, ZSST minus CONTROL, and ASYM are respectively represented in *magenta*, *red* and *blue thick line*. *Blue dashed line* is ASST minus CONTROL, ASST being described in Sect. 4.3. Square points represent values statistically significant at the 95 % of the student test

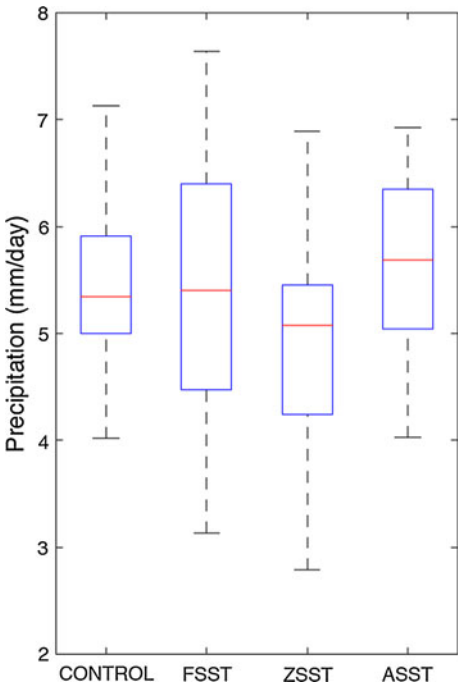

Fig. 10 Inter-member dispersion *boxplots* for rainfall mean of CONTROL, FSST, ZSST and ASST experiments, considering the SESA domain (32°S:25°S,60°W:50°W). On each box, the central mark is the median, the edges of the box are the 25th and 75th percentiles (*lower* and *upper* quartiles), and the whiskers mark the most extreme data

changes in the tropical ocean conditions and the rainfall response over South America.

Zonal mean meridional streamfunction changes are firstly analyzed to assess changes in the global Hadley cell, as described in Sect. 4.1.

The zonal mean meridional circulation shows similar changes in ZSST (Fig. 12a) and in FSST (Fig. 7c), but the weakening of the winter Hadley cell is more pronounced in ZSST (Fig. 12a). The zonal mean precipitation changes from ZSST, FSST and ASYM are presented in Fig. 12c. In agreement with the changes identified in the meridional circulation, both ZSST and FSST simulations show a precipitation increase along the ascent branch and a decrease over the southern descent region (Fig. 12c), where the subsidence is reinforced (Fig. 12a). These precipitation changes are larger in ZSST than in FSST. On the other hand, ASYM shows weaker changes in the meridional circulation (Fig. 12b). It is interesting to note that SST changes corresponding to ASYM do not directly include global warming forcing, since the global average of those SST changes is zero (Fig. 3c). The characteristics similar to those of the global warming represented in FSST, as for example the slowdown of the zonal Hadley circulation (see Sect. 4.1), are then only represented by ZSST, and with larger magnitude. Therefore, changes in large-scale atmospheric circulation associated with ASYM are not particularly expected. However, Fig. 12b shows a weak intensification of both the winter and summer Hadley cells in ASYM (increases of absolute values). A southward extension of the ascending zone of the winter Hadley cell is also obvious, in agreement with the negative precipitation change at about 3°S and a peak of precipitation increase at about 15°S (Fig. 12c). This result shows that the zonal mean meridional circulation in ASYM is mainly influenced by changes situated in the tropical Indian-western Pacific Ocean, where a southward shift of the ITCZ is clearly displayed (Fig. 11b). Consequently, the changes found in FSST (Fig. 12a) and ASYM (Fig. 12b) are of different nature. ASYM changes are associated with circulation changes induced by structural SST changes, not associated with the global mean SST warming as in ZSST, but with

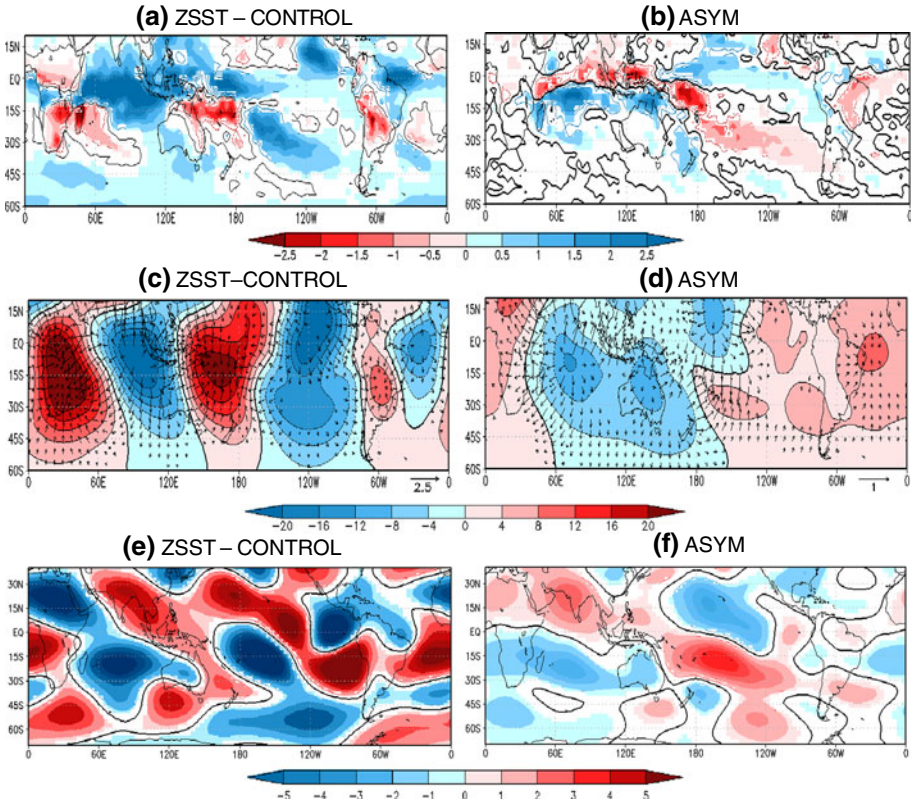

Fig. 11 *Top panels* **a** and **b** same as Fig. 8c, d, but for global rainfall anomalies. *Middle panels* 200-hPa velocity potential anomalies from LMDZ-global outputs (*contour* and *color*) and divergent wind (*vectors*) corresponding to **c** ZSST minus CONTROL, **d** ASYM. *Color* scale and *contour* interval is 4×10^5 m^2 s^{-1}. *Black thick contour* indicates the 0 level. Reference vector is displayed at the *lower right corner* in m s^{-1}. *Bottom panels* Zonal deviation of the 200-hPa streamfunction anomalies from outputs of LMDZ-global for **e** ZSST minus CONTROL, **f** ASYM. Values statistically significant at the 95 % of the student test are shaded. *Color scale* and *contour* interval is 1×10^6 m^2 s^{-1}. *Black contour* indicates the 0 level

changes in the physical mechanisms distinctive of each tropical region. Results also show that ZSST and ASYM display opposite changes of the winter Hadley circulation, in intensity as well as in location. This result agrees with those obtained by Gastineau et al. (2009) who performed similar numerical sensitivity simulations to structures of longitudinal and zonal SST changes using the IPSL-CM4 GCM, as it was described in Introduction.

Changes in the velocity potential and divergent wind at 200-hPa level are depicted in Fig. 11c, d. ZSST shows similar changes to FSST (Fig. 7b), with an intensified three-wave structure displayed (Fig. 11c). In contrast, ASYM shows anomalies of smaller magnitude, but with a one-wave structure, indicating an intensified upper-level divergence over the Indian-Western Pacific Oceans and an enhanced upper-level convergence over the rest of the tropical band with largest values over northeastern South America (Fig. 11d). This structure is similar to the long-wave regime pattern described by Chen et al. (1999), maintained by heating over the tropical Indian and western Pacific. In particular, ASYM exhibits a positive divergence anomaly over the Indian Ocean coherently with positive rainfall (Fig. 11d) and positive SST anomalies (Fig. 2c) over the same region. It is evident that the SST anomaly pattern, identified by Junquas et al. (2012) as the structure linked to rainfall increase over SESA, resembles that associated with the Indian Ocean Dipole (IOD) positive phase with positive anomalies in the western Indian Ocean and negative anomalies in the eastern part of the basin (e.g., Saji et al. 1999). Recently Cai et al. (2011a) analyzed WCRP/CMIP3 MME simulations and concluded that models with larger IOD amplitude, systematically produce larger rainfall change in IOD affected regions, linked to stronger teleconnections between IOD and rainfall anomaly regions. SESA has been identified as one of the IOD influenced regions in which positive IOD phases induce positive rainfall anomalies (Chan et al. 2008). The IOD-like structure, obvious in ASYM, is believed to contribute to the signal of SESA rainfall increase (Fig. 8d).

The atmospheric circulation rotational component, as described by the 200-hPa streamfunction anomalies (zonal mean removed) is displayed in Fig. 11e and f. The tropical and subtropical circulation response associated with both ZSST and ASYM, resembles the typical Gill pattern in response to a tropical diabatic heating, with upper-level anticyclonic (cyclonic) anomalies located poleward of the positive (negative) rainfall change regions (Fig. 11a, b). Furthermore, both ZSST and ASYM exhibit evidences of wave trains extended along the middle and high latitudes. Streamfunction anomalies for both ZSST and ASYM are associated with a wave number 2–3 pattern at around 50°S. ASYM shows, however, a distinctive cyclonic anomaly center over the subtropical central south Pacific, anticyclonic anomalies over the Indian Ocean and Australia

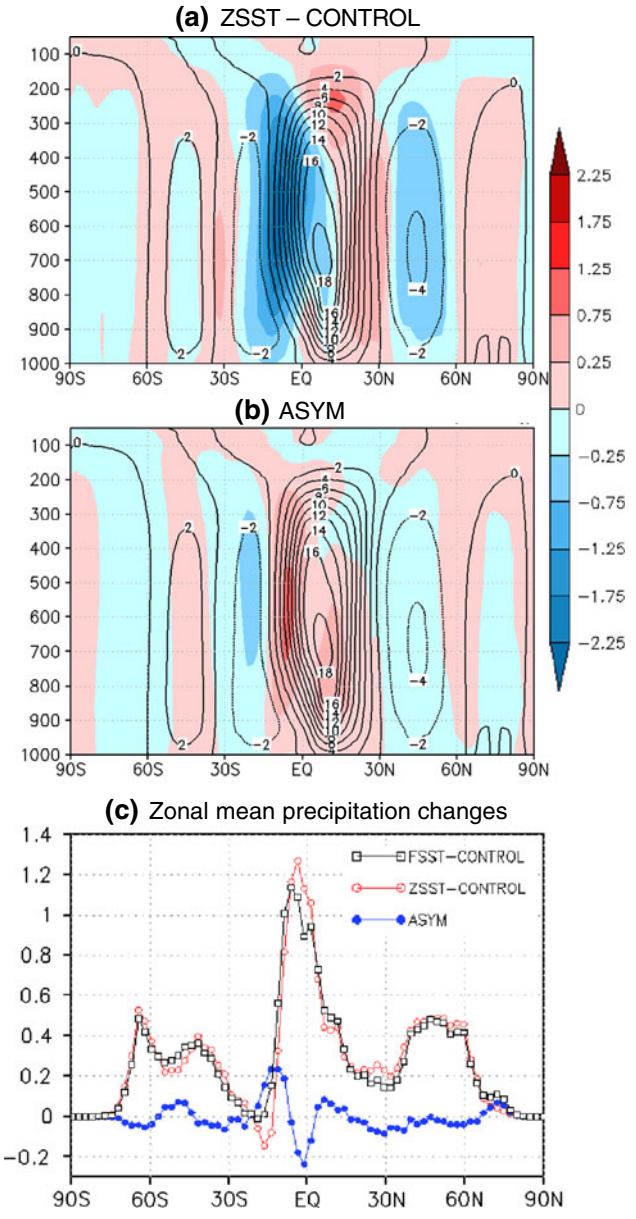

Fig. 12 Meridional streamfunction anomalies from LMDZ-global model corresponding to **a** ZSST minus CONTROL, **b** ASYM (*shaded* with a *color* scale interval of 0.25×10^{10} kg s^{-1}). The meridional streamfunction of the CONTROL experiment is represented in *black contours* with an interval of 2×10^{10} kg s^{-1}. **c** Zonal mean precipitation anomalies corresponding to FSST minus CONTROL (*black line*), ZSST minus CONTROL (*red line*), ASYM (*blue line*). Units: mm/day

(Fig. 11f). There is also clearly a wave-train like structure extended from the southwestern South Pacific along an arch trajectory towards South America. Chan et al. (2008) and Cai et al. (2011b), among others, have identified similar wave-train like structures linking both the Indian-western Pacific Ocean and the central Pacific Ocean with South America, in association with IOD and ENSO activities. Over South America, ZSST and ASYM induce circulation anomalies of opposite sign, being anticyclonic (cyclonic) over SESA and cyclonic (anticyclonic) over the SACZ region, respectively.

The origin of the wave-train identified along the South Pacific in ASYM (Fig. 11f) is further explored through an analysis of the 500-hPa geopotential height anomalies and the associated wave activity fluxes (computed as in Vera et al. 2004). Figure 13 confirms that the wave-train pattern extended along the South Pacific towards South America is mainly maintained by energy dispersion from the subtropical western Pacific, the maximum of the Rossby-wave source term being situated southeastwards of the maritime continent.

Regional atmospheric circulation changes in South America simulated by ZSST and those represented by ASYM are further explored through the analysis of the vertically-integrated moisture fluxes (Fig. 8g, h). A visual inspection shows that patterns of changes induced by ZSST (Fig. 8g) are similar to those induced by FSST (Fig. 8e). However, a more detailed analysis through the ASYM difference (Fig. 8h) shows an anticyclonic anomaly extended between SESA and the SACZ region that favors moisture convergence in SESA and divergence in the SACZ region. The latter contributes to the development of the rainfall dipole-structure (Fig. 8d). Such an anticyclonic eddy is similar to that found by Junquas et al. (2012) from WCRP/CMIP3 models for future climate projections, and to that found in observations of twenty century climate (e.g., Robertson and Mechoso 2000) in association with the rainfall anomaly dipole.

4.4 Linearity of the response

From the previous discussion, it seems that the rainfall increase projected for SESA in a future climate change scenario might result from the atmospheric circulation anomalies induced by the zonally asymmetric changes of the tropical SST. That influence was assessed in this work by analyzing the difference between FSST and ZSST (ASYM, see Sect. 2.2). Therefore, the issue about how linear the atmospheric response is to changes in the SST forcing is further explored in this section. Accordingly, an additional set of simulations was performed, forcing the model with the SST change resulting from the difference between the full and zonal average fields of the SST change projected by the WCRP/CMIP3 MME (Sect. 2.2) and represented in Fig. 2c. The run is called "ASST" and it was performed using the same methodology as for FSST and ZSST simulations (Table 2; Sect. 2.2). This run has the lower inter-member dispersion among all the experiments performed (not shown). The changes resulting from the difference between ASST and CONTROL simulations are compared to those obtained with ASYM. Consequently, the linearity of the atmospheric response is evaluated by

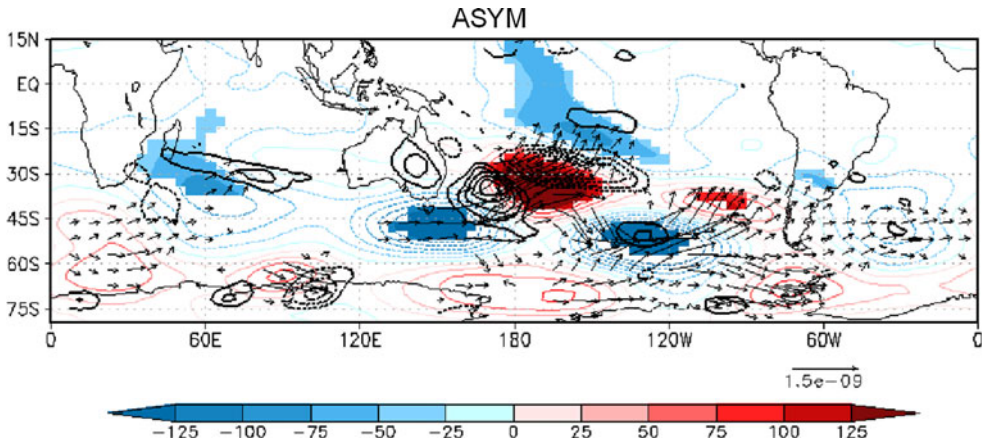

Fig. 13 500-hPa geopotential height anomalies from outputs of LMDZ-global for ASYM. *Values* statistically significant at the 95 % of the student test are *shaded*. *Color scale* and contour interval is 25 m^2 s^{-2}. *Vectors* represent horizontal wave flux activity based on the 500-hPa geopotential height anomalies. Reference vector of 2×10^{-9} m^2 s^{-3} is displayed at the *lower right corner*. *Thick black contours* are the Rossby wave source term, with interval of 0.2×10^{10} s^{-2} and the zero level omitted

comparing the changes induced by the same SST anomalies simulated in two different ways. If the atmospheric response is linear, the two signals should show similar changes.

Figure 14a, b display regional and global precipitation changes as obtained in ASST and they are compared to those associated with ASYM (Figs. 8d, 11b). It seems evident, not only for South America but also at global scale, that rainfall change patterns in ASST are similar to those in ASYM, confirming that a large degree of linearity exists in terms of large and regional atmospheric responses. The spatial distribution of ASST rainfall anomalies along the SESA-SACZ transect (Fig. 9) shows also coherent behavior with ASYM. In particular, ASST shows positive anomalies over SESA and negative anomalies in the SACZ region, as in ASYM. Positive SESA rainfall changes in ASST (Fig. 14a) seem located southwards, as compared to ASYM (Fig. 8d). A northward displacement of the Atlantic ITCZ is also obvious in ASST, and with stronger values than in ASYM. Considering all South America, statistical dispersion values between ASST and ASYM show close similarities, with a spatial correlation of 0.59 and a relative RMSE of about 6 % (half the value between GPCP and CMAP, see Table 3). Since there is no global SST change in ASST, it is clear that the precipitation increase found in SESA (Fig. 14a) is not the consequence of a global SST warming. We can reasonably argue that the similar signal found in ASYM (Fig. 8d) must be primarily due to the asymmetric part of the SST changes rather than a global warming SST. However, the magnitude of rainfall anomalies over both SESA and all South America in ASST is weaker than in ASYM (not shown). This could be due to the fact that the model is forced with smaller SST anomalies in ASST than in FSST and ZSST. Consequently, the positive (negative) change in SESA (SACZ) seems more pronounced when a global SST warming is added to such longitudinal asymmetric SST anomalies.

At global scale, main rainfall changes reproduced in ASST (Fig. 14b) are similar to those in ASYM (Fig. 11b). The spatial correlation between Figs. 14b and 11b is of 0.63. In particular, ASST also shows maximum values over the equatorial Indian-western Pacific Oceans, with negative anomalies over the equatorial Indian Ocean, and negative anomalies over the southern tropical Indian Ocean. However, some non-linear manifestations are also notable in those regions, represented by large differences between ASST and ASYM (Fig. 14c). It can be noticed that these regions have the warmest climatological SST (not shown) and thus host intense convective activities, which can be considered as a non-linearity source. In addition, those regions also correspond to maximum inter-member dispersion in ASST (not shown).

The 500-hPa geopotential height response in ASST was also examined (not shown). Rossby wave-trains emanating from the western tropical Indian and Pacific towards the SH extratropics are noticeable in ASST as well as in ASYM (Fig. 13), showing a large linearity. However, the circulation anomalies situated over both subtropical and tropical South America in ASST are located southwards from those displayed in ASYM. Such differences in circulation anomaly locations might explain the southward position of SESA rainfall anomaly found in ASST (Fig. 14a), when compared to ASYM (Fig. 8d). This result confirms the coherence of the physical mechanisms simulated by the model in response to the asymmetric SST change.

5 Summary and conclusion

Numerical simulations were performed with the TWN LMDZ4 system to explore mechanisms controlling the rainfall changes projected in South America in association

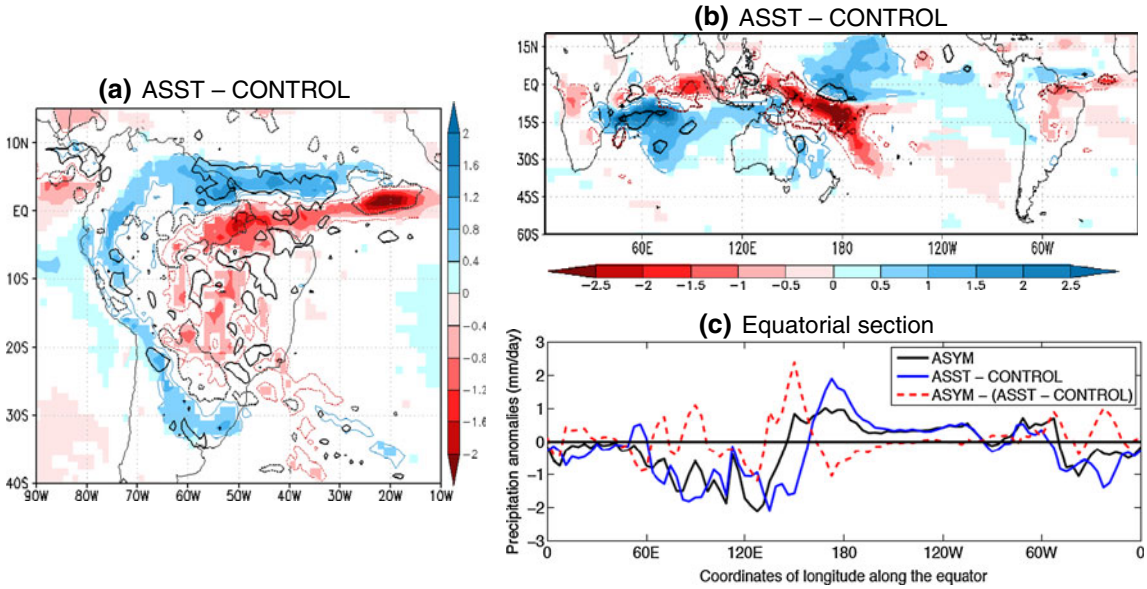

Fig. 14 Rainfall anomalies induced by ASST minus CONTROL from **a** LMDZ-regional outputs (interval is 0.4 mm/day), and **b** LMDZ-global outputs (interval is 0.5 mm/day). Values statistically significant at the 95 % of the student test are shaded. The ASYM minus (ASST minus CONTROL) difference is displayed in contours (interval is 1.5 mm/day, zero level omitted). **c** Zonal transect at 1°S of the rainfall anomalies induced by ASYM (*black line*), ASST minus CONTROL (*blue line*) and the difference between ASYM and ASST minus CONTROL (*dashed red line*). Data are from LMDZ-global outputs. Units are mm/day for all panels

with future SST changes. The TWN system coupling the regional and the global models shows in general a better representation of the climate in South America, compared to the global model operating alone. LMDZ4 under the TWN mode, is able to reproduce the main large-scale features of precipitation and atmospheric general circulation. The main model bias is associated with the representation of the convection over the maritime continent split in two separated regions, while observations show one contiguous rainfall region. It is likely that this bias is related to the low resolution of LMDZ-global model operating in this region under the TWN system. Previous studies showed that this region is particularly influent over the global climate (e.g., Lorenz and Jacob 2005). Also, Wu and Kirtman (2007) pointed out that the Asian-Australian monsoon variability may be dominated by atmospheric forcing, and thus the performance of SST-forced simulation can be particularly low in this region.

The numerical simulations performed confirm that the SST changes projected by the WCRP/CMIP3 models by the end of the twenty-first century induce significant variation in the climate of South America. Sensitivity simulations with different combinations of SST spatial patterns were performed to evaluate the role of different SST conditions in affecting rainfall variation in South America and the associated mechanisms. In particular, the SST change pattern was decomposed into two configurations: (1) zonal-mean meridional pattern representing the latitudinal component of the global SST change, essentially characterized by a stronger warming in equatorial oceanic regions than in the off-equatorial region, and (2) zonally-asymmetric pattern representing the longitudinal component of the global SST change, mainly characterized by a stronger SST increase in the equatorial Indian-western Pacific Oceans than in the rest of the equatorial band. Under such a configuration, the global average associated with the longitudinal component is zero and thus this component is not a global SST warming, but an associated asymmetric pattern.

The analysis of the simulations for the zonal-mean SST changes reveals an intensification of precipitation over the equatorial regions, where the SST warming is larger. In particular, an associated enhancement of the convection over the Atlantic ITCZ is found. Moisture transport from the equatorial Atlantic into subtropical South America decreases, the continental moisture gyre is reduced, and the humidity transport from the Amazon basin toward SESA weakens. We can also observe an intensification of the South Atlantic trade winds and an enhancement of the South Atlantic anticyclone, which increases the moisture transport in the northern part of the SACZ. Moreover, an anomalous subsidence that compensates the increased ascent in the ITCZ and SACZ region also contributes to inhibit precipitation in SESA. The atmospheric changes provoked by the zonal-mean SST changes are then favorable for a rainfall increase in the SACZ region, and a rainfall decrease in SESA.

On the contrary, the analysis of simulations for the asymmetric SST changes shows that the SST increase in

the Indian and equatorial western Pacific, which is the main feature of the zonally asymmetric SST change in the tropics, influences the SESA rainfall changes. The asymmetric SST changes induce anomalous atmospheric upper-level divergence over the Indian-tropical western Pacific Oceans, accompanied with an intensified subsidence particularly visible over the SACZ region. Such an anomalous divergence is the source for a Rossby wave-train pattern extending from the tropical western Pacific to South America, favoring a cyclonic circulation anomaly in the South of the continent, which in turn promotes humidity flux convergence (divergence) and an increase (decrease) of rainfall in SESA (SACZ). Consequently, the asymmetric pattern of the SST changes in the tropics seems to explain the projected DJF rainfall increase in SESA by the end of the twenty-first century. However, a global mean SST increase in combination with the asymmetric SST anomalies seems to accentuate that positive rainfall trend.

In order to assess the role of the direct radiative effects of the GHG increase, a simulation combining GHG increase and full SST changes was also performed. Results showed that SESA rainfall increase is mainly related to SST changes and not significantly affected by the radiative effects of the GHG increase. In addition, SESA rainfall change seems mainly related to the asymmetric SST changes, which are not directly linked to the global warming itself. Consequently, a consideration of the direct radiative influence of the GHG increase in the atmosphere does not seem very relevant in our simulations.

Results showed that in general the atmospheric responses to zonal and asymmetric SST changes exhibit opposite behaviors. The zonal SST change induces a weakening and poleward extension of the winter Hadley cell, that was also found as global warming consequence by most of the models in previous publications (e.g., Vecchi and Soden 2007; Lu et al. 2007; Gastineau et al. 2008). In particular such a Hadley cell expansion in South America is linked to an enhanced ITCZ over the tropical Atlantic and a decrease of precipitation in the subtropical regions of the continent. Therefore, this result tends to suggest that the global-scale atmospheric circulation changes in relation to the zonal-mean SST changes are not relevant in explaining the rainfall increase in SESA. A rainfall decrease is even expected for this region. On the other hand, the asymmetric SST change is related to a reinforcement of the atmospheric general circulation (Hadley and Walker), and a southward displacement of the ascending motion, mostly explained by changes in the Indian and western Pacific tropical regions. Precipitation increase in SESA represented by the asymmetric SST changes seems mainly explained by remote influences from the western Pacific, via teleconnection processes associated with Rossby wave-trains.

SESA gives a striking example showing that precipitation projections at regional scale can strongly depend on the mechanisms of teleconnection between the global and regional climate, as simulated by models. In that sense, it is interesting to note that the LMDZ4 model was able to simulate two coherent behaviors with relevant large-scale and regional mechanisms explaining two opposite rainfall changes in SESA. The two SST forcings were then in combination to explain the full SST change: (1) the zonal-mean SST change inducing a rainfall decrease in SESA, and (2) the asymmetric SST change inducing a rainfall increase in SESA. The full SST change simulation showed that changes in LMDZ4 are dominated by the zonal SST change forcing, inducing a decrease of rainfall in subtropical-tropical SESA. This is coherent with the coupled model IPSL-CM4 employing LMDZ4 for its atmospheric component, which shows a negative precipitation trend in SESA. Such behavior could be at least partially due to the fact that the associated SST change pattern projected by IPSL-CM4 (Fig. 1a of Gastineau et al. 2009), shows a much smaller asymmetry signal between the tropical Pacific and tropical Atlantic than that displayed by the full SST change pattern considered in this study (Fig. 2a). This suggests that the zonal SST change forcing could dominate the signal in IPSL-CM4.

With the same SST change configuration as used in this paper, Junquas et al. (2012) found that all the 9 WCRP/CMIP3 models with a projected SESA rainfall increase showed the mechanism of Rossby-wave teleconnection. It is not known if the projected changes in these 9 models are influenced by both signals of zonal and asymmetric forcings as in LMDZ4. We don't know neither what are their relative contributions to the final signal. However, the physical mechanism outlined in Junquas et al. (2012) as being associated with the positive rainfall SESA projection are similar to those associated with the asymmetric forcing in LMDZ4. In that sense, it could be speculated that the asymmetric part of SST change was the dominant forcing for these models. It is, however, necessary to use one or more of these models with a similar experimental protocol to confirm the hypothesis.

Changes in SESA rainfall strongly depend on the way that mechanisms of teleconnections are reproduced by models, and how much each process dominates the model responses to future global warming. It is then crucial to include the relevant physical mechanisms of teleconnection in order to do a reliable regional-scale climate projection. Moreover, the fact that both large-scale and regional circulation changes have been identified as relevant in explaining the mechanisms associated with rainfall increase in SESA, confirms the importance of using an atmospheric global model and a regional model with two-way-nesting configuration, in order to represent not only

the regional influences, but also the teleconnections between the tropics and the region. Future investigations with WCRP/CMIP5 SST changes should be pursued to confirm the results.

Acknowledgments Comments and suggestions provided by three anonymous reviewers were very helpful in improving this paper. We acknowledge the international modeling groups for providing their data for analysis, the Program for Climate Model Diagnosis and Intercomparison (PCMDI) for collecting and archiving the model data, the JSC/CLIVAR Working Group on Coupled Modeling (WGCM) and their Coupled Model Intercomparison Project (CMIP) and Climate Simulation Panel for organizing the model data analysis activity, and the IPCC WG1 TSU for technical support. The IPCC Data Archive at Lawrence Livermore National Laboratory is supported by the Office of Science, U.S. Department of Energy. This research was supported by the European Commission's Seventh Framework Programme (FP7/2007-2013) under Grant Agreement N° 212492 (CLARIS LPB. A Europe-South America Network for Climate Change Assessment and Impact Studies in La Plata Basin), CNRS/LEFE Program, and CONICET PIP 112-200801-00399. The first author C.J. is supported by a Ph.D grant from the Ecole Polytechnique.

References

Allen MR, Ingram WJ et al (2002) Constraints on future changes in climate and the hydrologic cycle. Nature 419:224–232

Barreiro M, Tippmann A (2008) Atlantic modulation of el nino influence on summertime rainfall over southeastern south America. Geophys Res Lett 35:L16704. doi:10.1029/2008GL035019

Barros V, Doyle M, Camilloni I (2008) Precipitation trends in southeastern south America: relationship with Enso phases and with low-level circulation. Theor Appl Clim 93:19–33

Cai W, Sullivan A, Cowan T, Ribbe J, Shi G (2011a) Simulation of the Indian Ocean dipole: a relevant criterion for selecting models for climate projections. Geophys Res Lett 38:L03704. doi:10.1029/2010GL046242

Cai W, van Rensch P, Cowan T, Hendon HH (2011b) Teleconnection pathways of ENSO and the IOD and the mechanisms for impacts on Australian rainfall. Bull Am Meteorol Soc 24:3910–3923

Chan SC, Behera SK, Yamagata T (2008) Indian Ocean dipole influence on South American rainfall. Geophys Res Lett 36:L14S12. doi:10.1029/2008GL034204

Chen T, Weng S, Schubert S (1999) Maintenance of austral summertime uppertropospheric circulation over tropical south America: the bolivian high-nordeste low system. J Atmos Sci 56:2081–2100

Chen W, Jiang Z, Li L, Yiou P (2011) Simulation of regional climate change under the IPCC A2 scenario in southeast China. Clim Dyn 36:491–507

Chou C, Neelin JD (2004) Mechanisms of global warming impacts on regional tropical precipitation. J Clim 17:2688–2701

Christensen JH, Hewitson B, Busuioc A, Chen A, Gao X, Held I, Jones R, Kolli RK, Kwon W-T, Laprise R, Magaña Rueda V, Mearns L, Menéndez CG, Räisänen J, Rinke A, Sarr A, Whetton P (2007) Regional climate projections. In: Solomon S, Qin D, Manning M, Chen Z, Marquis M, Averyt KB, Tignor M, Miller HL (eds) Climate change 2007: the physical science basis. Contribution of working group I to the fourth assessment report of the intergovernmental panel on climate change. Cambridge University Press, Cambridge

Codron F, Sadourny R (2002) Saturation limiters for water vapour advection schemes: impact on orographic precipitation. Tellus A 54:338–349

Collins M, An S, Cai W, Ganachaud A, Guilyardi E, Jin F, Jochum M, Lengaigne M, Power S, Timmermann A et al (2010) The impact of global warming on the tropical pacific ocean and el niño. Nat Geosci 3:391–397

Doyle M, Barros V (2002) Midsummer low-level circulation and precipitation in subtropical south America and related sea surface temperature anomalies in the south Atlantic. J Clim 15:3394–3410

Gastineau G, Le Treut H, Li L (2008) Hadley circulation changes under global warming conditions indicated by coupled climate models. Tellus A 60:863–884

Gastineau G, Li L, Le Treut H (2009) The hadley and walker circulation changes in global warming conditions described by idealized atmospheric simulations. J Clim 22:3993–4013

Gates WL (1992) AMIP: the atmospheric model intercomparison project. Bull Am Meteorol Soc 73:1962–1970

Grimm A, Barros V, Doyle M (2000) Climate variability in southern south america associated with el niño and la niña events. J Clim 13:35–58

Hoffman J (1975) Maps of mean temperature and precipitation. Clim Atlas S Am 1:1–28

Hourdin F, Musat I, Bony S, Braconnot P, Codron F, Dufresne J, Fairhead L, Filiberti M, Friedlingstein P, Grandpeix J (2006) The lmdz4 general circulation model: climate performance and sensitivity to parametrized physics with emphasis on tropical convection. Clim Dyn 27(7):787–813

Huffman GJ, Bolvin DT, Adler RF (2011) GPCP version 2.2 combined precipitation data set. WDC-A, NCDC, Asheville, NC. Data set accessed at http://www.ncdc.noaa.gov/oa/wmo/wdcamet-ncdc.html

IPCC (2007) Summary for policymakers. In: Solomon S, Qin D, Manning M, Chen Z, Marquis M, Averyt KB, Tignor M, Miller HL (eds) Climate change 2007: the physical science basis. Contribution of working group I to the fourth assessment report of the intergovernmental panel on climate change. Cambridge University Press, Cambridge

Junquas C, Vera C, Li L, Le Treut H (2012) Summer precipitation variability over southeastern south America in a global warming scenario. Clim Dyn 38:1867–1883

Krishnamurti T, Kanamitsu M, Koss W, Lee J (1973) Tropical east-west circulations during the northern winter. J Atmos Sci 30:780–787

Labraga J, Frumento O, López M (2000) The atmospheric water vapor cycle in south America and the tropospheric circulation. J Clim 13:1899–1915

Li Z (1999) Ensemble atmospheric GCM simulation of climate interannual variability from 1979 to 1994. J Clim 12:986–1001

Lorenz P, Jacob D (2005) Influence of regional scale information on the global circulation: a two-way nesting climate simulation. Geophys Res Lett 32:L18706. doi:10.1029/2005GL023351

Lu J, Vecchi GA, Reichler T (2007) Expansion of the hadley cell under global warming. Geophys Res Lett 34:L06805. doi:10.1029/2006GL028443

Marengo J, Soares W, Saulo C, Nicolini M (2004) Climatology of the low-level jet east of the andes as derived from the NCEP-NCAR reanalyses: characteristics and temporal variability. J Clim 17:2261–2280

Marti O et al (2005) The new IPSL climate system model: IPSL-CM4. Note du Pôle de Modélisation No. 26. Institut Pierre Simon Laplace des Sciences de l'Environnement Global, Paris. http://dods.ipsl.jussieu.fr/omamce/IPSLCM4/DocIPSLCM4/FILES/DocIPSLCM4.pdf

Paegle J, Mo K (2002) Linkages between summer rainfall variability over south America and sea surface temperature anomalies. J Clim 15:1389–1407

Robertson A, Mechoso C (2000) Interannual and interdecadal variability of the south Atlantic convergence zone. Mon Weather Rev 128:2947–2957

Saji NH, Goswami BN, Vinayachandran PN, Yamagata T (1999) A dipole mode in the tropical Indian Ocean. Nat 401:360–363

Simmons A, Uppala S, Dee D, Kobayashi S (2006) Era-interim: new ecmwf reanalysis products from 1989 onwards. ecmwf, shinfield park. Reading, Berkshire RG2 9AX, UK, 25

Sörensson A, Menéndez C, Samuelsson P, Willén U, Hansson U (2010) Soil-precipitation feedbacks during the South American monsoon as simulated by a regional climate model. Clim Change 98:429–447

Sugi M, Yoshimura J (2004) A mechanism of tropical precipitation change due to CO_2 Increase. J Clim 17:238–243

Takahashi K, Battisti DS (2007) Processes controlling the mean tropical Pacific precipitation pattern. Part I: the Andes and the eastern Pacific ITCZ. J Clim 20:3434–3451

Tanaka H, Ishizaki N, Kitoh A (2004) Trend and interannual variability of walker, monsoon and hadley circulations defined by velocity potential in the upper troposphere. Tellus A 56:250–269

Vecchi G, Soden B (2007) Global warming and the weakening of the tropical circulation. J Clim 20:4316–4340

Vecchi G, Soden B, Wittenberg A, Held I, Leetmaa A, Harrison M (2006) Weakening of tropical pacific atmospheric circulation due to anthropogenic forcing. Nat 441:73–76

Vera C, Silvestri G, Barros V, Carril A (2004) Differences in el nino response over the southern hemisphere. J Clim 17:1741–1753

Vera C, Higgins W, Amador J, Ambrizzi T, Garreaud R, Gochin D, Gutzler D, Lettenmaier D, Marengo J, Mechoso C, Nogues-Paegle J, Silva Diaz PL, Zhang C (2006a) Towards a unified view of the American monsoon system. J Clim 19:4977–5000

Vera C, Silvestri G, Liebmann B, González P (2006b) Climate change scenarios for seasonal precipitation in south America. Geophys Res Lett 33:L13707. doi:10.1029/2006GL025759

Wu R, Kirtman B (2007) Regimes of seasonal air–sea interaction and implications for performance of forced simulations. Clim Dyn 29:393–410

Xie P, Arkin P (1997) Global precipitation: a 17-year monthly analysis based on gauge observations, satellite estimates, and numerical model outputs. Bull Am Meteorol Soc 78:2539–2558

Xu H, Wang Y, Xie S-P (2004) Effects of the Andes on eastern Pacific climate: a regional atmospheric model study. J Clim 17(3):589–602